

**This is a non-peer reviewed pre-print.**

The Manuscript is currently under review in Marine and Petroleum Geology. Please note the subsequent version of this manuscript may have a different content.

# **Multiple episodes of sand injection leading to accumulation and leakage of hydrocarbons along the San Andreas/San Gregorio fault system, California.**

Giuseppe Palladino<sup>1,2\*</sup>, Roberto Emanuele Rizzo<sup>1</sup>, Gustavo Zvirtes<sup>1</sup>, Antonio Grippa<sup>1</sup>,  
Andrew Hurst<sup>1</sup>, Ruy Paulo Philipp<sup>4</sup>, David Healy<sup>1</sup> and G. Ian Alsop<sup>1</sup>

<sup>1</sup>Department of Geology and Petroleum Geology, School of Geosciences, University of Aberdeen, Aberdeen, UK

<sup>2</sup>Dipartimento di Scienze, Università degli Studi della Basilicata, Potenza, Italy

<sup>4</sup>Departamento de Mineralogia e Petrologia, Universidade Federal do Rio Grande do Sul, Porto Alegre, Rio Grande do Sul, Brazil

\*Corresponding author: Giuseppe Palladino, E-mail: Giuseppe.palladino@abdn.ac.uk

## **1 Abstract**

2 The presence of sand injections has proven to enhance the likelihood of hydrocarbon traps  
3 within siliciclastic successions. Through the development of large interconnected networks of  
4 sills and dykes, sand injection complexes provide a volume of porous and permeable rocks  
5 within the low permeability host units. Overall, the formation of sand injection complexes  
6 requires extensive fracturing and hydrofracturing, which can be particularly pronounced when  
7 sand injections are coupled with brittle tectonic deformation. In exceptional circumstances,  
8 this process may threaten the integrity of the reservoir top seal thereby preventing further  
9 hydrocarbon accumulation. Studying exceptional exposures along the coastal area of Santa  
10 Cruz in California, we report evidence for top seal failure associated with injection episodes.  
11 Two distinct sand injection episodes are proposed. A first event, datable to Late Miocene,  
12 allowed for large volumes of sand to be emplaced within the top-seal units followed by  
13 accumulation of hydrocarbons within newly injected sandstones. Later, a series of brittle  
14 tectonic events, associated with San Andreas/San Gregorio Fault System, caused

15 remobilisation and accumulation of sand along newly formed fault planes. This combination  
16 of pervasive brittle deformation and sandstone injection along fault structures, as this detailed  
17 case study documents, can disrupt the integrity of a host unit, leading to the overall failure of  
18 a top seal and leakage of hydrocarbons.

19

20 Keywords: Sandstone intrusions; Santa Cruz Injection Complex; Santa Cruz petroleum  
21 system; Sandstone-filled faults; Hydrocarbon leakage; San Andreas/San Gregorio fault  
22 system; California.

23

## 24 **1. Introduction**

25 Fracturing and faulting processes associated with emplacement of sandstone intrusions  
26 in the shallow crust are caused either by an excess of pore-fluid pressure, or regional tectonic  
27 stresses, and are among the main mechanisms responsible for top seal failure in sedimentary  
28 successions where sands alternate with low-permeability mudstones (Hurst et al., 2011). In  
29 particular, hydrofracturing and faulting processes related to fluid overpressure commonly  
30 initiate at the interface between the reservoir rocks and top seal strata, when fluid pressure  
31 exceeds the fracture gradient and then propagates throughout the top seal sequence (Jolly and  
32 Lonergan, 2002). Fractures and faults related to regional tectonic stresses commonly involve  
33 the entire reservoir/top seal system and, also, cut through the interface separating the two  
34 different portions (Palladino et al., 2018).

35 In general, brittle deformation processes associated with emplacement of sandstone  
36 intrusions can lead to either the partial or the complete breaching of the sealing sequence, with  
37 two contrasting outcomes for oil retention: i) partial top seal breaching generally will result in  
38 enhanced reservoir capacity, as fault and fracture apertures, together with highly-permeable  
39 sandstone intrusions, provide new capacity for hydrocarbon accumulation; ii) alternatively,

40 complete breaching of the sealing sequence will prevent hydrocarbons accumulation due to  
41 bypass mechanisms or, in the case that hydrocarbons are already accumulated in the reservoir,  
42 lead to leakage phenomena (Cartwright et al., 2007).

43         Given the potential importance of the above relationships, the study of the interactions  
44 between faults, fractures and sandstone intrusions cannot be ignored when exploring for  
45 hydrocarbon reservoirs. In this work, we present direct field evidence for top seal failure  
46 associated with emplacement of sandstone intrusions forming the Santa Cruz Injection  
47 Complex (SCIC) in the coastal area of California (Thompson et al., 2007) (Fig. 1). The SCIC  
48 shares its main elements with other sand injection complexes in California (e.g. Vigorito and  
49 Hurst, 2010; Scott et al., 2013) displaying a complete suite of components which comprise a  
50 source rock, an intrusive network, and an extrudite complex (Scott et al., 2009). The SCIC is  
51 part of the Santa Cruz petroleum system, thereby representing an ideal analogue for  
52 hydrocarbon-bearing sand injections in the subsurface (Dixon et al., 1995; Duranti et al., 2002;  
53 Duranti and Hurst, 2004). The first studies describing sand injections in the Santa Cruz area,  
54 date back to the beginning of the 20<sup>th</sup> century (Eldridge, 1901; Newsom, 1903) and focused  
55 on the potential of mining these tar-sand deposits. After tar production decreased, successive  
56 studies focussed on the mechanisms leading to the emplacement of sandstone intrusions, and  
57 on the relationships between sand injections and tectonic structures in the area (Phillips, 1990;  
58 Molyneux, 1999; Boehm and Moore, 2002; Jolly and Lonergan, 2002; Thompson et al., 2007;  
59 Scott et al., 2009; Sherry et al., 2012). Based on contradictory field evidence, which indicates  
60 the contemporaneous occurrence of sandstone intrusions emplaced along faults, and sandstone  
61 intrusions overprinted by tectonic structures, two main mechanisms invoking episodes of  
62 pore-fluid overpressure, and tectonic processes were formulated. It is important to note that  
63 in both cases, the resulting models considered that the SCIC was emplaced as a single event.

64           In this study we have undertaken a detailed geological survey along the coastal sector  
65 between Santa Cruz and Davenport (Fig. 1) and have focussed on the cross-cutting  
66 relationships between sandstone intrusions and tectonic structures in the SCIC. This outcrop-  
67 based investigation allowed us to recognise that the present architecture of the SCIC is a  
68 consequence of a two-stage injection. During the first stage, which occurred in the Late  
69 Miocene, the partial failure of the top seal leads to the emplacement of sandstone intrusions  
70 within the Santa Cruz Mudstone. The high resealing capacity of the system at this time  
71 allowed successive hydrocarbon accumulation. During the second stage, sandstones intruded  
72 along high angle extensional faults associated with the San Andreas/San Gregorio fault  
73 system. The age of this later event is not well-constrained, although must have occurred  
74 between the Late Miocene and the Quaternary and caused the leaking of hydrocarbons  
75 previously accumulated in the system. The main aims of this work are: i) to present evidence  
76 for two different sandstone injection stages leading to the building of the SCIC; ii) to discuss  
77 the relationships between tectonic structures and sandstone intrusions, and provide clear field  
78 descriptions about the cross-cutting relationships occurring between the two recognised  
79 events; iii) to propose an evolutionary model showing the initiation, development and the  
80 successive failure of the of Santa Cruz petroleum system.

81

## 82   **2. Geological setting**

### 83   *2.1 Geology of the Santa Cruz coastal area*

84           The coastal sector between the City of Santa Cruz and Davenport is part of the "Ben  
85 Lomond domain" (*sensu* Aydin and Page, 1984), which is a relatively undeformed area  
86 between the two major San Andreas and San Gregorio dextral strike-slip fault zones  
87 (Dickinson et al., 2005) (Fig. 1a-c). The outcrops consist of a Middle Miocene-Pliocene

88 sedimentary succession unconformably overlying the granitic/metamorphic Salinian  
89 basement, which forms the southwest flank of the Ben Lomond Mountain (Clark, 1981; Page  
90 et al., 1998) (Fig. 1d). The base of the sedimentary succession consists of shallow-marine  
91 arkosic sandstone of the Middle Miocene Lompico Formation, which rests unconformably  
92 upon the crystalline basement. This formation reaches a maximum thickness of about 240m  
93 and is conformably overlain by bathyal biosiliceous mudrocks and sandstones of the Monterey  
94 Formation (Clark, 1981). The Monterey Formation reaches a thickness of 800m in the study  
95 area and is unconformably overlain by the Santa Margarita Sandstone (Fig. 1d). This  
96 formation consists of coarse-grained, large-scale cross-bedded arkosic sandstones and fine-  
97 grained bioturbated sandstones, deposited in a tidal/nearshore depositional environment. The  
98 unit has a maximum thickness of 130m and the coarse-grained facies contain accumulations  
99 of oil and tar. The Santa Margarita Sandstone is considered to be the reservoir of the Santa  
100 Cruz petroleum system, whereas the Monterey Formation represents the source rock (see the  
101 next section). The Santa Cruz Mudstone stratigraphically overlies the Santa Margarita  
102 Sandstone (Fig. 1d), and consists of organic-rich, thickly bedded, biosiliceous mudstone and  
103 thin porcelanite layers containing dolomite and calcite concretions. Green mudstone horizons  
104 up to 10 cm thick locally alternate with the previously described mudstone lithologies. The  
105 Santa Cruz Mudstone was deposited in a shelf environment approximately 9.0–7.0 Ma ago  
106 (Barron, 1986) and reaches a maximum thickness of 2700m. It is considered to be the top seal  
107 for the Santa Cruz petroleum system. The Purisima Formation is the youngest unit recognised  
108 in the Santa Cruz area. It consists of Miocene to Pliocene, very thick-bedded tuffaceous and  
109 diatomaceous siltstones alternating with thick-bedded andesitic sandstones, deposited in a  
110 neritic environment which in places reaches 300m in thickness.

111 The Santa Cruz succession forms the southwestern flank of the of the Ben Lomond  
112 mountain fold (Stanley and McCaffrey, 1983) which is a southeast-plunging anticline formed

113 between the San Andreas and San Gregorio fault zones (Fig. 1b). Other important tectonic  
114 structures in the area are the Ben Lomond and Zayante fault zones (Clark and Rietman, 1973,  
115 Clark, 1981, Brabb, 1989) (Fig. 1b).

116 Displacement across the Pacific-North America transform margin has been slightly  
117 compressive since 8 Ma (Atwater and Stock, 1998), resulting in a progressive tectonic uplift  
118 of the area marked by folding and faulting. In particular, a series of NW-SE trending anticlines  
119 and synclines formed between the Zayante/Ben Lomond fault system and the San Andreas  
120 Fault whereas, west of the Ben Lomond fault, a gently SW-dipping homocline forms the major  
121 structure in the study area. Uplift in the Santa Cruz area has been continuous between the late  
122 Tertiary and Quaternary, with a calculated uplift rate of 0.16 m/1,000 yr (Bradley and Griggs,  
123 1976). More recently Bürgmann et al. (1994) suggested an average uplift rate of the order of  
124 0.8 mm/yr over the last 4.6 m.y. The SCIC is currently exposed along wavecut platforms and  
125 cliffs in the Santa Cruz Mudstone, located on the southwestern side of Ben Lomond Mountain.

126

## 127.2. *The Santa Cruz petroleum system*

128 The Santa Cruz petroleum system (SCPS) is a fossil petroleum system that displays a  
129 complete sequence of source rock, reservoir, top seal, and overburden represented by the  
130 Monterey, Santa Margarita Sandstone, Santa Cruz Mudstone and Purisima formations,  
131 respectively (Phillips, 1990; Hosford Scheirer et al., 2013) (Fig. 1d). Petroleum generation  
132 occurred during a narrow span of time between 7Ma and 5Ma (Hosford Scheirer et al., 2013).  
133 Although the Monterey Formation is considered to be the source rock for the SCPS,  
134 geochemical studies suggest that the Santa Cruz Mudstone is another possible petroleum  
135 source (Lillis and Stanley, 1999). SCPS mainly consists of tar-saturated sandstones, with oil  
136 and gas recognised in the Santa Cruz Mountain area and also along the coast. Hydrocarbons  
137 represented by both oil and gas are also present offshore along the Santa Cruz continental

138 margin (Mullins and Nagel, 1982; Heck et al., 1990). In the coastal area, the reservoir rocks  
139 mainly consist of heavy oil and tar-saturated sandstones irregularly distributed in an area of  
140 about 120 km<sup>2</sup> included between Davenport, Bonny Doon and Santa Cruz (Fig. 1). Tar-  
141 saturated sandstones and hydrocarbon seeps occurring in the Santa Cruz coastal area are well-  
142 known since the end of the 19th century (Eldridge, 1901; Newsom, 1903; Jenkins, 1930), and  
143 attained moderate economic significance following the 1906 earthquake in San Francisco  
144 when sand from the Santa Margarita Sandstone was mined to provide asphalt for road  
145 rebuilding. In the same area, the occurrence of petroleum has also been ascertained and  
146 estimates of oil reserves varied from 10 million bbl to 20 million bbl which classifies the SCPS  
147 as a minor oil field (Page and Holmes, 1945; Phizackerley and Scott, 1978; Hallmark, 1980).  
148 Although the Santa Cruz petroleum system has only limited economic relevance, the  
149 significance of its study lies in the fact that it represents a valid analogue for larger subsurface  
150 oil fields.

151

### 152 **3. The Santa Cruz Injection Complex**

#### 153 *3.1 Factors controlling emplacement, geometry and architectural organization of sandstone* 154 *intrusions*

155 Sandstone intrusions originate by the forceful emplacement of fluidised sand into an  
156 actively propagating hydraulic fracture system within low permeability host rocks. Pore-fluid  
157 pressure must exceed the fracture toughness of the host strata. Additionally, to mobilise sand  
158 from unconsolidated parent depositional units the velocity of the pore-fluid must exceed the  
159 minimum fluidisation velocity (Lowe, 1975). For fine- to medium grained sand the minimum  
160 fluidisation velocity is estimated to range between 0.001 ms<sup>-1</sup> and 0.01 ms<sup>-1</sup>, although during  
161 large-scale injection much higher velocity is inferred (Duranti and Hurst, 2004; Hurst et al.,

162 2011). Pore-fluid is generally driven upward following the pressure gradients that form  
163 between high-pressured zones in the shallow crust, typically at depths of less than 1.5 km  
164 burial and the Earth's surface (Vigorito and Hurst, 2010; Hurst et al., 2011).

165 Variations in pore-fluid pressure within the host strata and the underlying pressure cell  
166 typically form sandstone intrusion complexes that consist of four main architectural elements  
167 comprising the parent units, dikes, sills and extrudites (Vigorito and Hurst, 2010) (Fig. 2a).  
168 The distribution and geometry of sandstone intrusions in the crust are generally the result of  
169 the interaction between pore-fluid pressure and the lithostatic pressure (overburden). For  
170 example, sills mainly develop at a depth where the fluid pressure is equal or greater than the  
171 lithostatic pressure (lithostatic equilibrium surface, LES of Vigorito and Hurst, 2010) forming  
172 a sill zone in which the greatest volume of injected sand occurs (Fig. 2a). Dikes dominate  
173 immediately above the parent units (the lower dike zone) and between the sill zone and the  
174 sand extrudites (upper dike zone) (Fig. 2a). Unlike other sandstone intrusion complexes  
175 occurring in central California (i.e. the Panoche Giant Injection Complex of Vigorito and  
176 Hurst, 2010) the SCIC does not show a vertical and lateral continuity due to tectonic  
177 disturbance. However, the different architectural elements are still recognisable in different  
178 outcrops exposed along the Santa Cruz coastal area.

179 The distribution and geometry of sandstone intrusions also depends on whether  
180 dominant regional tectonic stress fields are developed. Based on natural examples, and  
181 laboratory experiments which modelled unconsolidated homogeneous material as the host  
182 unit, it has been demonstrated that intrusions tend to fill pre-existing tectonic structures, and  
183 that they predominantly form low to high angle dikes in tectonically active areas (Galland et  
184 al., 2003; 2007; Ferre' et al., 2012; Palladino et al., 2016; 2018) (Fig. 2b). Flat-lying intrusive  
185 geometries are still possible in compressional settings when the maximum principal stress ( $\sigma_1$ )  
186 is horizontal and the minimum principal stress ( $\sigma_3$ ) is vertical.

187           The SCIC extends for 15 km between the city of Santa Cruz and Davenport and for  
188 several km inland (Fig. 1). It consists of three different architectural elements termed the  
189 parent units, the intrusive network, and extrudites that will be described in the following  
190 sections. We also include sandstone intrusions within the SCIC that are emplaced along faults  
191 and are not temporally correlated with the majority of sandstone intrusions recognised in the  
192 study area.

193

### 194 *3.2. Parent units*

195           Although the parent-intrusion relationships are typically not well exposed, the Santa  
196 Margarita Sandstone is generally interpreted to be a parent unit (Boehm and Moore, 2002;  
197 Thompson et al. 2007). Multiple parent sandstone units were invoked by Clark (1981) for the  
198 SCIC using mineralogical data from exposures at Panther Beach/Yellowbank Creek localities  
199 (Fig. 1). The Pliocene Purisma Formation was identified as a parent unit based on similar  
200 overall composition and the occurrence of andesine feldspar, which has a volcanic provenance  
201 and is unknown in the Santa Margarita Sandstone (Scott et al., 2009). For the Purisima  
202 Formation (Early Pliocene; Norris, 1986) to form a parent unit would require its juxtaposition  
203 below the Miocene Santa Cruz Mudstone at the time of sand injection. This would have  
204 occurred not earlier than the earliest Pliocene and implies that the large intrusions at Panther  
205 Beach/Yellowbank Creek were not emplaced until then. Unfortunately, the poor lateral  
206 exposure of the SCIC combined with sparse biostratigraphic control and, very limited  
207 mineralogical data from the Santa Margarita Sandstone, compromise interpretation.

208

### 209 *3.3. The intrusive sand network*

210           The SCIC has a widespread and well-developed intrusive network, which mainly  
211 consists of dikes and occasional sills. Saucer-shaped intrusions are also locally present. Single  
212 intrusions generally range from a few centimetres to a decimetre thick, while isolated dikes or  
213 sills can locally be several metres thick. Although the distance from one large intrusion to  
214 another can be significant (in the order of tens or hundreds of metres), the presence of minor  
215 intrusions provides good connectivity throughout the injection network. Connectivity between  
216 sandstone intrusions is demonstrated by the common occurrence of tar that has migrated along  
217 the fractures cropping out in study area.

218

### 219 *3.3.1. Dikes*

220           Dikes are very well exposed in the study area, with key localities at 4 Mile Beach and  
221 Bonny Doon (Fig. 1). Within the general Santa Cruz coastal area, dikes are sub-vertical, or at  
222 high angles to bedding, and occur as single intrusions or swarms that are water and tar  
223 saturated (Fig. 3a-e). Single dikes vary in aperture from a few centimetres to more than 1m.  
224 Bifurcation (Fig. 3a), side-stepping and marked changes in orientation are common (Fig. 3b,  
225 c). Dikes are typically planar with sharp discordant margins with host strata, although  
226 undulating, irregular contacts also occur, usually in association with intensely fractured zones.  
227 Mudstone clasts of host strata commonly form “floating” textures in a sandstone dike matrix.  
228 These clasts are generally angular to slightly rounded and jigsaw textures occur (Duranti and  
229 Hurst, 2004) (Fig. 3d-e). The internal structure of the sandstone intrusions is characterised by  
230 mm- to cm-spaced banding. Dikes fall into three main trends that are oriented N-S, WSW-  
231 ENE and SW-NE (Fig. 3f).

232

### 233 *3.3.2. Sills*

234 Sills mainly crop-out at Panther Beach/Yellowbank Creek, while small-scale sills also  
235 occur at 4 Mile Beach (Fig. 1). Sills typically display low-angle ( $<5^\circ$ ) discordance with  
236 bedding (Fig. 4), and range in thickness from a few centimetres to several decimetres, with  
237 the exception of the Panther Beach/Yellowbank Creek locality where sills are up to ~20m in  
238 thickness (Thompson et al., 2007; Scott et al., 2009) (Fig. 1). Sill margins are irregular with  
239 lateral thickness variation and abrupt lateral terminations. The lower contacts of sills are often  
240 erosive with scoured surfaces common, while upper boundaries are commonly discordant with  
241 the host strata (Fig. 4a, b). These sharply discordant erosive contacts with overlying host strata  
242 conclusively demonstrate the intrusive origin of the sills. Meter to 10's of meters wide convex-  
243 up features, termed scallops (Hurst et al., 2005), are sometimes associated with dikes that  
244 emanate from them into the overburden. Mudstone breccias with jigsaw configuration of  
245 clasts, together with isolated mudstone rafts, occur along the upper and lower margins of sills.  
246 Internal sedimentary structures are dominated by mm- to dm-thick banding, which is oriented  
247 approximately parallel to the margins of the sandstone intrusions. Plane-parallel and cross-  
248 lamination are also commonly observed. Within the thickest sills, sedimentary features  
249 including convolute lamination, fluid-escape structures and pipes suggest turbulent flow  
250 during emplacement (Scott et al., 2009).

251

### 252 *3.3.3. Saucer-shaped intrusions*

253 Saucer-shaped, tar-saturated sandstone intrusions are very well exposed at 4 Mile  
254 Beach (Fig. 1). In cross-section, they consist of an inner bedding-parallel sandstone intrusion  
255 that are connected laterally with two outer sills by means of segments inclined at between  $15^\circ$   
256 and  $60^\circ$ . Similar features observed on seismic images are often referred to as wings (Huuse et  
257 al., 2007, Jackson et al., 2011). Inner sills, that are typical of large saucer-shaped intrusions,  
258 are not observed (Huuse et al., 2007; Hurst and Vigorito, 2017). The saucer-shaped sandstone

259 intrusions coalesce to form a composite intrusion with “petals of a flower” geometry, which  
260 are connected by smaller, contemporaneous dikes. Bifurcation and convergence of the saucers  
261 is characteristic (Fig. 4c, d). A nested geometry of saucers occurs where smaller intrusions  
262 overlie large saucers and are linked by dikes with cusped geometry (Fig. 4e, f). Saucer-shaped  
263 intrusions are 2 to 15 cm thick with undulating, stepped margins. Although sandstone  
264 intrusions probably comprise less than 10% of the rock volume they provide excellent  
265 connectivity as demonstrated by the pervasive tar saturation.

266

#### 267 *3.3.4 Sandstone-filled faults*

268 Sandstone intrusions emplaced directly along tectonic structures are a volumetrically  
269 small, and therefore frequently overlooked, characteristic of sandstone intrusion complexes  
270 (Palladino et al., 2016, 2018). In the SCIC, they are an integral part of the injection complex  
271 and predominantly consist of sandstone-filled normal faults (SFNF *sensu* Palladino et al.,  
272 2018) with sandstone intrusions along strike-slip and compressional faults planes less  
273 common. Sandstone-filled normal faults (SFNF) are cm- to dm-wide, with small offsets,  
274 rarely developed shear zones and steeply-dipping attitude.

275 Sandstone-filled normal faults are well exposed at Bonny Doon and Laguna Creek  
276 beaches (Fig. 1). At Bonny Doon Beach, a series of N-S and NNW-SSE oriented SFNF form  
277 a conjugate set that dissect the Santa Cruz Mudstone (Fig. 5a); a thin mudstone interval forms  
278 a useful marker bed (Fig. 5b). The master fault consists of a high angle SFNF with a maximum  
279 thickness of 30 cm and a throw of 15 cm. The entire exposure of the fault is propped open by  
280 a sandstone fill. A weak damage zone, consisting of closely-spaced fractures, occurs parallel  
281 to the fault margin. Unlike associated faults that are not intruded by sandstone and contain a  
282 fault gouge comprising cataclastic breccia and clay smear, the SFNF commonly lacks of fault  
283 gouge.

284 At Laguna Creek Beach the outcrop has numerous normal fault planes that are characterised  
285 by intense cataclasis and clay smearing with occasional SFNF present. An almost vertical fault  
286 zone displays the ~50 cm offset of a clay marker bed (Fig. 5c, d). The fault consists of two  
287 main fully-injected overlapping segments, which are connected by secondary *en echelon*  
288 linked fractures (Fig. 5e, f). Locally, these linked fractures have a sandstone fill. Most of  
289 deformation is confined between the two fault segments whereas the external areas have very  
290 little evidence of brittle deformation. The role played by these structures in the evolution of  
291 the Santa Cruz petroleum system, and the relationships between sandstone-filled faults and  
292 the other elements of the SCIC are discussed in detail later.

293

### 294 3.4 Sand extrudites

295 Remarkable exposure of several sand extrudites at Red, White and Blue Beach (Fig.  
296 1) records at least three, and probably four, phases of sand extrusion onto a stacked series of  
297 paleo-seafloors (Fig. 6). They occur as tar-saturated, laterally-discontinuous, mounded  
298 sandstone units within the Santa Cruz Mudstone that are temporally and spatially distinct  
299 (Hurst et al., 2006). Extrudites extend over hundreds of meters, are meters thick, and consists  
300 of sand bodies that display a well-developed bed-parallel lamination or cross-bedding (Fig.  
301 6a, b). Locally, the original structure of sand volcanoes, which show multiple conduits and  
302 laminated flanks reaching inclinations approaching 30°, are still preserved. Planar basal  
303 surfaces are common, disturbed only by occasional sub-vertical “escape” burrows and, by the  
304 occurrence of sandstone-filled pockmarks. The pockmarks are underlain by dykes that  
305 terminate at the paleo-seafloor and are typically <5 m across although one >30 m wide  
306 pockmark is preserved, which is fed by numerous low- and high-angle to bedding dykes.

307

## 308 4. Tectonic structures in the Santa Cruz area

309           In order to investigate the relationships that exist between tectonic structures and  
310 sandstone intrusions, a detailed structural survey has been carried out in five key outcrop  
311 locations: Shark Fin Cove, Bonny Doon Beach, Laguna Beach, Panther Beach and 4 Mile  
312 Beach (Fig. 1c). Tectonic structures mainly consist of large-scale open folds, meso-scale  
313 faults, and dilatant fractures and joints. According to our observations and those of previous  
314 studies (Phillips, 1990), the structures are interpreted as a brittle expression of the Cenozoic  
315 tectonic deformation related to the San Gregorio and San Andreas faults (Fig. 1a, b).

316

#### 317 *4.1. Folds*

318           Open anticlinal and synclinal folds with decametre to kilometre wavelength are  
319 recognised throughout the study area (Fig. 7a, b). They are characterised by gently-dipping  
320 limbs and fractured fold hinges. In outcrop, the fold hinge zone is often removed by erosion.  
321 Fold axes commonly display NW-SE trends and SE plunges, which is in general agreement  
322 with observations made by Phillips (1990) (Fig. 7c).

323

#### 324 *4.2. Faults*

325           Sets of differently oriented faults are the most prominent tectonic feature recognised  
326 along the coastal sector (Fig. 8a). Normal faults are the most common fault type, while strike-  
327 slip and occasional reverse faults are less common.

328           In general, normal faults consist of conjugate sets with a master fault plane and a series  
329 of minor associated antithetic and synthetic faults and fractures. Usually, major structures  
330 have small offsets, ranging from a few centimetres to some metres, and form a graben-like  
331 geometry (Fig. 8b). The best exposures of normal faults are found at 4 Mile Beach, Laguna  
332 Creek Beach and Bonny Doon Beach (Fig. 8c). Normal fault kinematics are characterised by

333 dip-slip oriented slickensides coupled with stratigraphic offsets. Fault zones are commonly  
334 marked by fault breccia, together with fine-grained cataclastic crushed material. Clay smear  
335 is locally observed along the fault planes where they cut clay-rich horizons (Fig. 8d).

336 In common with the normal faults, strike-slip (Fig. 8e, f) and reverse faults (Fig. 8g,  
337 h) are characterised by limited displacement and narrow fault zones are best exposed around  
338 4 Mile and Bonny Doon beaches. Fault breccia is rarely present, although thin (cm-scale)  
339 cataclastic zones and striated fault planes occur locally.

340 Measurement of fault orientation at all locations allows us to identify several fault sets  
341 that display a range of orientations and kinematics. In general, conjugate sets of NNE-SSW,  
342 N-S, NNE-SSW and NE-SW trending faults consist of extensional faults, NW-SE and NNW-  
343 SSE trending faults comprise dextral strike slip faults, and E-W and WNW-ESE trending  
344 structures have a less clear kinematic origin.

345

#### 346 *4.3. Fractures*

347 Fractures form a pervasive network throughout the study area. In general, fracture  
348 density increases from centimetres to a few millimetres when approaching fault planes.  
349 Conversely, fractures are regularly distributed and more widely spaced (centimetres to a few  
350 tens of centimetres) in the intra-fault areas (Rizzo et al., 2017). Outcrops at 4 Mile and Panther  
351 beaches (Fig. 1) represent typical case study fracture scenarios for the studied area.

352 The cliff-line of 4 Mile Beach is an excellent location for the study of fracture  
353 geometry, and the interactions between fractures and sandstone intrusions. In particular, most  
354 of the outcrop consists of steep, vegetation-free walls and a series of raised, intertidal terraces  
355 that together provide an exceptional ‘pseudo-three dimensional’ outcrop. Fractures are  
356 generally connected by abutments (Y- or T- points *sensu* Manzocchi et al., 1998 and  
357 Manzocchi, 2002) or have cross-cutting relationships (Fig. 9a). Fracture length varies from a

358 few centimetres to some decimetres, with an average length in the order of 20 cm (Rizzo et  
359 al., 2017). Fracture apertures average on the order of 3 ( $\pm 2$ ) mm. Linkages between different  
360 fractures occur by dilatational jogs, horsetail and, without any physical intersection, by means  
361 of *en echelon* arrays (Kim et al., 2004; Peacock et al., 2016). In cross-section, the fractures  
362 usually show X and S shaped geometries (Fig. 9b). Fracture meshes (Sibson, 1996) are also  
363 common (Fig. 9c). Observations of plumose structures with well-developed hackle fringes  
364 support the hypothesis that Mode I tensile fracturing is the main mechanism by which  
365 fractures opened. Local evidence for shear fracture mechanisms is provided by calcite-filled  
366 tension gashes. As fractures cross different lithologies, diffraction phenomena may occur.  
367 Commonly, tensional fractures are filled by a hydrocarbon residue of tar (Rizzo et al., 2017)  
368 (Fig. 9d), together with less common calcite infill (Fig. 9e). Fracture distribution at 4 Mile  
369 Beach has two major conjugate fracture sets trending NNW-SSE and NW-SE (Fig. 9f).

370 At Panther Beach (Fig. 1), closely-spaced fractures are well-exposed along a series of  
371 cliff sections that are similar to those at 4 Mile Beach. Here, the thick sandstone sill  
372 (Thompson et al., 2007; Scott et al., 2009) (Fig. 4a) shows a different style of fractures, with  
373 X-shaped geometry and mm-thick deformation bands, that isolate rhomboidal segments of  
374 sandstone (Fig. 9g). Millimetre-scale offsets typify fracture intersections. Fractures either  
375 terminate along, or are deflected by, finer grained, clay-rich layers. The fracture distribution  
376 displays predominantly NNW-SSE-orientations, with NW-SE-oriented fractures also  
377 abundant, while NE-SW and E-W-striking trends are less evident (Fig. 9h).

378

#### 379 *4.4. Origin of tectonic structures in the Santa Cruz area*

380 Studies of Pliocene-Quaternary tectonic structures in the San Francisco Bay area,  
381 which includes the Santa Cruz area, were performed by a number of authors (Wilcox et al.,  
382 1973; Aydin and Page, 1984; Page et al., 1998). Based on these studies, the orientations of the

383 tectonic structures recognised in the study area are consistent with a "wrench tectonic"  
384 environment (Moody and Hill, 1956) developed under the control of the San Andreas (average  
385 azimuth N324°) and the San Gregorio (average azimuth N341°) dextral strike-slip fault zones  
386 (Aydin and Page, 1984; Phillips, 1990) (Fig. 1b). Orientations of tectonic structures measured  
387 in the Santa Cruz coastal area show a close similarity with those predicted by the model.  
388 However, comparison between outcrop fault orientations with those produced in laboratory  
389 experiments also identified some inconsistencies (Aydin and Page, 1984). Primarily, these  
390 inconsistencies are attributable to the orientation of tectonic structures not being the result of  
391 movement along a single major fault, but rather the result of different interacting major faults.  
392 Secondly, fault orientation also depends on the mechanical behaviour of the different  
393 lithologies undergoing deformation. Finally, fracture orientation is affected by crustal  
394 heterogeneity and rotation during progressive shear.

395 The main ranges of fault trends recognised in the Santa Cruz Coastal area are  
396 illustrated in Fig. 10. NW-SE and NNW-SSE trending faults are interpreted as conjugate sets  
397 of strike-slip faults developed parallel to the San Andreas and the San Gregorio fault zones,  
398 whereas NNE-SSW oriented strike slip faults correspond to the associated Riedel structures  
399 (Fig. 8e, f). NNW-SSE, N-S, NNE-SSW and NE-SW trending extensional faults are dilational  
400 step-overs between right-lateral faults (Fig. 8b, c).

401 Unlike extensional and strike slip faults, SW-NE and WSW-ENE trending  
402 contractional faults (Fig. 8g, h) are inconsistent with a wrench tectonic model. However, they  
403 could be an expression of compressional deformation connected with the development of the  
404 Santa Cruz homocline between the Ben Lomond Mountains and the San Gregorio Fault  
405 (Stanley, 1990). According to Phillips (1990), southwest-plunging folds may be related to  
406 differential compaction mechanisms between thick sedimentary beds of the Santa Margarita  
407 Sandstone and the overlying Santa Cruz Mudstone.

408 Fracture orientations largely reflect the trends of the main faults. For example, at 4 Mile and  
409 Panther beaches (Fig. 9), most of the N-S, NNE-SSW and NE-SW oriented fractures are  
410 consistent with the dominant extensional fault trends throughout the area. Similarly, NNW-  
411 SSE and NW-SE fracture orientations are consistent with the dextral strike-slip faults. The  
412 NE-SW trends could however be associated with outer-arc axial fracturing related to the  
413 folding phase. As fractures that accompany the emplacement of the sandstone intrusions are  
414 distributed along well-defined trends, we exclude a possible hydraulic fracturing origin that  
415 would typically show less constrained orientations.

416

## 417 **5. Relationships between sandstone intrusions and tectonic structures**

418 In the previous sections we described the main characteristics and spatial distribution  
419 of sandstone intrusions and tectonic structures occurring in the Santa Cruz coastal area. Field  
420 observations allowed us to recognise sandstone intrusions that are either related or unrelated  
421 to tectonic structures that are now discussed.

422

### 423 *5.1. Sandstone intrusions associated with tectonic structures*

424 Close relationships between sandstone intrusions and tectonic structures have already  
425 been ascertained by the recognition in the study area of sandstone-filled normal faults  
426 (Phillips, 1990; Palladino et al., 2018) (Fig. 5). This evidence clearly indicates that fluidised  
427 sand was driven along tectonic discontinuities. The influence of tectonics on the distribution  
428 of sandstone intrusions is evident when comparing dike orientations with fault and fracture  
429 patterns (Fig. 11). Although sandstone dikes are spatially more dispersed than the orientation  
430 of the major faults, their orientation follow broadly similar trends of NNW-SSE, N-S, SW-  
431 NE and WSW-ENE, which are consistent with the average fault and fracture orientations.

432 Notably, all dominant trends coincide with dilational structures. In particular, the majority of  
433 NNW-SSE, N-S and SW-NE oriented structures are compatible with extensional faults,  
434 whereas WSW-ENE oriented structures likely coincide with outer-arc extension fractures  
435 related to folding (Fig. 7). A small number of injections coincide with strike slip or  
436 contractional faults in which dilation is commonly inhibited.

437

#### 438 *5.2. Sandstone intrusions not associated with tectonic structures*

439 The occurrence of sandstone-filled faults and fractures noted above markedly contrasts  
440 with sandstone intrusions which are unrelated to tectonics (Thompson et al., 1999; Boehm and  
441 Moore, 2002, Scott et al., 2009). These intrusions are considered to be emplaced in  
442 propagating hydraulic fracture network systems that formed during periods of severe,  
443 sometimes supra-lithostatic, pore-fluid pressure in the very shallow crust (Hurst et al., 2011).  
444 These sand injections are clearly overprinted by tectonics and do not show intrusion-parallel  
445 fractures that would progressively increase toward dike margins, as expected for tectonically-  
446 related intrusive geological bodies (Delaney et al., 1986). Evidence for tectonic overprint of  
447 sandstone intrusions are particularly well-exposed at 4 Mile Beach, Shark Fin Cove and  
448 Laguna Beach.

449 At 4 Mile Beach, saucer-shaped sandstone intrusions are intensely overprinted by  
450 closely-spaced fractures which are genetically associated with larger extensional faults (Fig.  
451 12a, b). We found no evidence of hydrofracturing and polygonal faults (Cartwright et al.,  
452 2003; Vigorito et al., 2008; Vigorito and Hurst, 2010) that are generally invoked as the  
453 mechanism which accommodates the emplacement of sandstone intrusions in sedimentary  
454 basins unaffected by tectonic deformation. Fractures systematically cut through the sandstone  
455 intrusions and continue into the host strata, indicating that the deposits were well-lithified at  
456 the time when tectonic deformation occurred.

457           Of particular interest, is the 1.5 m thick sandstone dike cropping out in three adjacent  
458           locations at Shark Fin Cove (Fig. 12c). At two of the locations, the dike has planar margins,  
459           sharp contacts with the host strata, and no evidence of dike-parallel fracturing or mechanical  
460           brecciation, as typically associated with a fault plane (Fig. 12d). By contrast, at the third  
461           outcrop, the dike is significantly affected by post-emplacement deformation (Fig. 12e). In this  
462           case, deformation is concentrated along the dike margins, resulting in their reactivation.  
463           Occurrence of slickensides along the dike surfaces adds support to this interpretation. Here,  
464           stress concentration is accommodated differently by the mudstone and sandstone: in the brittle  
465           mudstone, deformation caused pervasive, intense fracturing that produced chaotic fine-  
466           grained cataclastic material; in the sandstone, deformation produces conjugate, widely-spaced  
467           fracture sets (Fig. 12f).

468           A 1.5 m wide dike at Laguna Beach (Fig. 1) has evidence of post-emplacement vertical  
469           compression associated with regional extensional faulting (Fig. 12g). Consequently, we can  
470           interpret the observed conjugate fractures and shear surfaces that dip at 45° from the vertical  
471           (Fig. 12h) as structures formed by a vertical maximum principle stress ( $\sigma_1$ ) that acted upon  
472           the poorly-consolidated sandstone. Prevailing arrays of NW-dipping shear planes caused the  
473           partial sinistral offset of the dike (Fig. 12h). In the mudstone host strata, brittle deformation  
474           mostly formed fractures, whereas in the sandstone deformation was accommodated mainly  
475           through conjugate deformation bands, with millimetres to centimetres offsets. When crossing  
476           the boundary separating the host strata from the dike, tectonic discontinuities are often  
477           refracted.

478

479           5.3. *Cross-cutting relationships*

480            Assuming a relatively synchronous faulting event in the Santa Cruz area, then the  
481            critical observations are: a) faults and associated fractures overprint and deform pre-existing  
482            sandstone intrusions, and, b) sand is injected along fault and fracture planes. These  
483            relationships make it unlikely that the SCIC was built during a single-stage emplacement  
484            event. Rather, the data shown in this work demonstrate that the present architecture of the  
485            SCIC results from distinct emplacement events. It follows that, two contrasting styles of sand  
486            injection are recorded in the Santa Cruz area, an earliest associated with hydraulic fracturing  
487            in the very shallow crust (<250 m burial, Vigorito and Hurst, 2010), that was followed by a  
488            later injection event guided by tectonics, cross-cutting the earlier intrusions suites. The same  
489            brittle deformation phase caused the definitive failure of the hydrocarbons top seal.

490            The early sandstone intrusions form an assorted suite consisting of both high and low-  
491            angle dikes, sills and saucer-shaped sandstone intrusions (Fig. 4). This event is recorded by  
492            several extrudites, whose origin is related to different pulses of sand mobilisation identified at  
493            different stratigraphic levels in the succession (Hurst, 2006) (Fig. 6). The second generation  
494            of sandstone intrusions is emplaced along pre-to-syn-tectonic structures,

495            Clear cross-cutting relationships between the two recognised generations of sandstone  
496            intrusions are well-exposed at Panther Beach (Fig. 13). Here, in the south-eastern side of the  
497            beach, the first generation of sandstone intrusions is cut by sandstone-filled faults (Fig. 13a).  
498            The outcrop consists of a cliff made of diatomaceous mudstone hosting a 10cm thick, tar-  
499            saturated, low-angle dike belonging to the first generation of sandstone injections (Fig 13b).  
500            The dike has a reasonably constant lateral thickness, internal sedimentary structures, as well  
501            as bed-parallel mm-thick banding and no evidence of hydrofracturing associated with its  
502            emplacement. The dike is repeatedly cut by a series of conjugate sandstone-filled normal  
503            faults (Fig. 13c) showing offsets of a few centimetres.

504           One of the through-going faults named Fault 1 (Fig. 13b), visible on the right-hand  
505 side of the outcrop, offsets the low-angle dike by about 10 cm. A closer caption of the fault  
506 plane (Fig. 13d) highlights a very complex geometry; it mainly consists of several fault planes  
507 connected by linking damage zones here represented by extensional fractures and dilatational  
508 jogs. Locally, these structures are filled by the sand which is likely to have been produced by  
509 the partial fluidisation of the faulted sand bodies. Where the fault intercepts the marker bed,  
510 the latter appears stretched and thinned rather than sharply cut by the tectonic structure. We  
511 can identify three different zones along the faulted dike. In the inner zone (Fig. 13 e, f), in the  
512 proximity of the fault plane, the sand is structureless and contains floating clasts derived from  
513 the host strata. This characteristic indicates that fluidization processes predominantly occurred  
514 during faulting in this portion. In the intermediate zone (Fig. 13 e, f), the dike is largely  
515 affected by fracturing (in a conjugate geometry) which overprints the original banding. Such  
516 features suggest that in this zone, the sand composing the dike was able to retain the tectonic  
517 structures and was not fluidised at the time of the deformation. In the external zone (Fig. 13  
518 e, f), the lack of deformation structures and the occurrence of well-preserved bed-parallel  
519 banding indicates that this zone was unaffected by deformation. This lateral distribution  
520 clearly suggests that the faulted sandstone dike behaves in a progressively more ductile  
521 manner approaching the fault plane. In contrast, the host rock shows a brittle behaviour as  
522 testified by the occurrence of pervasive fractures.

523           A second fault zone, named Fault 2 (Fig. 13g.), clearly offsets the low-angle dike  
524 however with a different deformation style compared to Fault 1. In this case there are no  
525 evidence of ductile deformation and sand remobilisation along the exposed section. However,  
526 syn/post-faulting sandstone intrusions occurred along a series of *en echelon* dilation fractures  
527 associated with the main fault plane (Fig. 13h, i). In this case, the fluidised sand might have  
528 been generated in distant portions of the fault and be laterally transported along dilatational jogs.

529           The last fault zone, named Fault 3 (Fig. 13k), consists of a steeply-dipping normal fault  
530           discontinuously filled by tar-saturated sandstone. The fault plane shows a stepped geometry  
531           and sandstone intrusions mainly occur in correspondence with releasing steps which form  
532           lozenge-shaped cavities (Fig. 13l). Sandstone intrusions are also present along vertical  
533           fractures and minor fault planes associated with the main structure. The sandstone-filled  
534           structure cuts the low-angle dike and the offset is about 10 cm.

535

## 536           **6. Discussion**

537           Previous attempts to comprehend both the potential of the Santa Cruz petroleum  
538           system (SCPS) and the distribution of the local paleo-stress have led to studies focussing on  
539           the organization of the SCIC, and the relationships between the sandstone intrusions and  
540           tectonic structures (Clark, 1981; Phillips, 1981; 1990; Thompson et al., 1999; Boehm and  
541           Moore, 2002). In most of these studies, the regional tectonic stresses were inferred to control  
542           the emplacement of sand injections, which, in turn, influenced hydrocarbon accumulation.  
543           Field observations clearly reveal that, in places, dikes are intruded along faults. Phillips (1981;  
544           1990) originally noticed the correspondence between fault and dike orientations, and therefore  
545           suggested that the emplacement of sandstone intrusions was mainly related to tectonic  
546           processes. Later, Thompson et al. (1999) confirmed the occurrence of sand injections along  
547           faults and fractures, however he also observed episodes of faulting that post-date sandstone  
548           intrusion at Yellowbank Creek. Boehm and Moore (2002) recognised a predominant NE-SW  
549           trend for the Santa Cruz sandstone intrusions, thus supporting the hypothesis of a strong  
550           tectonic control for sand injections. Similar to Thompson et al. (1999), they also provided  
551           evidence of faulting and fracturing that post-dates the sand injections. However, Boehm and  
552           Moore (2002) described a mechanical inconsistency represented by the emplacement of north-  
553           east-striking dikes, which would require a NW-SE minimum principal stress orientation ( $\sigma_3$ ),

554 and the simultaneous intrusion of sills, which suggests a sub-vertical minimum principal  
555 stress. The authors solved the apparent inconsistency proposing a model where dikes intruded  
556 perpendicularly to the NW-SE oriented  $\sigma_3$ , and simultaneously weak sediment cohesion of the  
557 host rock allowed sills to be emplaced parallel to bedding (i.e. pre-existing bedding-parallel  
558 weakness). Notably, these previous works considered the emplacement of the SCIC to be the  
559 result of a single injection event.

560 Based on the data presented in the previous sections, in particular on the detailed cross-  
561 cutting relationships, it is possible to explain the inconsistencies raised by Boehm and Moore  
562 (2002) in terms of a model involving two separate phases of sand injection from the Upper  
563 Miocene onwards (Fig. 14). Although these two events involved the same stratigraphic unit,  
564 i.e. the Santa Cruz Mudstone, the mechanical response of the sedimentary sequence and the  
565 regional tectonic controls varied between the two injection events thereby resulting in  
566 sandstone intrusions displaying different characteristics.

567 The first injection event (Fig. 14a) caused the partial fluidisation of the Santa Margarita  
568 Sandstone and the emplacement of a significant volume of remobilised sand into the overlying  
569 top seal unit represented by the Santa Cruz Mudstone. This injection event mainly led to the  
570 emplacement of sills, saucer-shaped intrusions and some low-angle dikes as seen at 4 Mile  
571 Beach and Panther Beach (Fig. 4). Isolated dikes locally connected flat-lying sandstone  
572 intrusions positioned at different stratigraphic levels in the Miocene succession.

573 The energy released during this event was large enough to create fluid-pressure  
574 gradients between buried sand bodies and the basin floor. This resulted in the development of  
575 a complete sand injection complex, spanning from remobilised parent units, intrusive  
576 elements to extrudites (Scott et al., 2009; Vigorito and Hurst, 2010). Sills and saucer-shaped  
577 intrusions were emplaced at the depth where the vertical pore-fluid pressure gradient is equal

578 to, or exceeds the overburden pressure, resulting in the minimum principal stress ( $\sigma_3$ ) being  
579 vertical.

580 Evidence for this first top seal failure event, and initiation of the sand injection  
581 complex, are provided by the internally-stacked, sheet or mounded sandstones at Red and  
582 White Blue Beach (Fig. 1), which are interpreted as extrudites (Boehm and Moore, 2002;  
583 Hurst et al., 2006). The series of three or four periods of extrusion are implicitly, and in some  
584 cases visibly, associated with underlying sand injection complexes that occurred during  
585 periods of otherwise fine-grained sedimentation, typically dominated by biosiliceous silica  
586 throughout the Late Miocene. The cyclic occurrence of extrudites in the mudstone succession  
587 reflects the alternating episodes of overpressure build-up and its subsequent release. In the  
588 field, no evidence for hydraulic fracturing attributable to this first event has been recognised.  
589 The lack of fractures is possibly related to the host strata still being poorly consolidated at the  
590 time of sand injection. If any fracture network did develop at this time, it behaved as a valve  
591 for the temporary passage of fluids and fluidised sands, thereby allowing overpressure to be  
592 dissipated. However, due to the unconsolidated state of the host unit, fractures were likely  
593 resealed soon after the sand emplacement thereby allowing the successive accumulation of  
594 hydrocarbon in the SCPS (Fig. 14b). In addition, once Opal A/Opal CT transformation  
595 involved the Santa Cruz Mudstone (El-Sabbagh and Garrison, 1990), most of the remaining  
596 fractures disappeared obliterating evidence of hydraulic fracturing processes.

597 Several factors, in addition to rapid burial and regional tectonics, may have contributed  
598 to the build-up of the necessary fluid pressure. According to laboratory experiments (Galland  
599 et al., 2003) (Fig. 2), the occurrence of flat-lying sandstone intrusions, as well as sill and  
600 saucer-shaped intrusions indicates the absence of oriented tectonic stresses, or, more probably,  
601 the development of a horizontal maximum principal stress which led to the folding of the  
602 Miocene succession. According to Phillips (1990), differential compaction and compressional

603 tectonics created folding suitable for hydrocarbon migration and accumulation. This event  
604 could have also triggered sandstone injections as many intrusions are concentrated along the  
605 crest of the anticlines (Thompson et al. 1999; Boehm and Moore, 2002). In this context, sand  
606 injections cropping out at Major Creek (Fig. 1), one of the most extensive injected sand bodies  
607 and previously exploited for tar mining, corresponds with the crest of a major SW-plunging  
608 anticline.

609           Following this event, the system resealed, and the depositional and injected sandstones  
610 collectively created a permeable network allowing further hydrocarbon accumulation.

611           The second injection event (Fig. 14c) caused sand fluidisation and remobilization of  
612 both the Santa Margarita Sandstone and the previously injected sandstone intrusions. The new  
613 sand injections mainly consist of a series of high angle dikes, emplaced along extensional  
614 faults and fractures, consistently following the trend of the San Andreas/San Gregorio fault  
615 system (Fig. 8), cutting through the Santa Cruz Mudstone that were by this time fully lithified.  
616 The sudden failure and re-opening of the system caused a rapid fluid transfer from the  
617 underlying overpressured units into the newly-formed structures, according to the mechanism  
618 proposed by Palladino et al. (2018). Sandstone-filled faults and brittle deformation  
619 accompanying this injection phase clearly post-date sandstone intrusions created during the  
620 first event (Fig. 13). We then suggest that this fault system reached the basin floor or the  
621 topographic surface breaking the top seal and triggering the consequent leak of the  
622 hydrocarbons. This chain of events is documented by the widespread occurrence of tar-  
623 saturated sandstones and fractures currently observed at Santa Cruz. Extrudites may also have  
624 been produced during this event but, unfortunately, recent erosional surfaces (Weber and  
625 Allwardt, 2001) cut the studied outcrops, and do not allow a precise age constraint for this  
626 faulting/injection event.

627

628 **7. Conclusions**

629 The acquisition of detailed structural data, together with observations of the  
630 relationships between the existing sedimentary and tectonic elements, allow us to unravel the  
631 evolutionary history of the Santa Cruz petroleum system (SCPS) in Central California. In  
632 particular, the evolution of the Santa Cruz petroleum system has been characterised by  
633 multiple episodes of sandstone intrusions by the Late Miocene onwards, which lead to  
634 emplacement of the Santa Cruz Injection Complex (SCIC). In this study sand injection  
635 episodes have been grouped into two main phases:

636 - During the first phase, the partial failure of the top seal, the Santa Cruz Mudstone, lead to the  
637 emplacement of a series of sills, saucer-shaped intrusions and dikes under the control of  
638 compaction and compressional tectonic processes. The new added sand enhanced the  
639 permeability of the Santa Cruz Mudstone and allowed hydrocarbon accumulation. The lack  
640 of brittle deformation features associated with this first event testifies that sand injection  
641 occurred in a poorly consolidated host rock (i.e. the Santa Cruz Mudstone) and that the  
642 fractures resealed soon after sand emplacement. The healing of the fracture system enabled  
643 the accumulation and entrapment of hydrocarbons, building of the Santa Cruz petroleum  
644 system. Sandstone extrudites allows us to attribute this event to the Late Miocene.

645 - The second phase of the sand injection was closely associated with brittle tectonic events, as  
646 well supported by the sand bodies emplaced along high-angle extensional faults. Brittle  
647 deformation accompanying this event indicates that sand injection occurred in well-  
648 consolidated host strata. This event, whose age is still uncertain, although it ranges between  
649 the Late Miocene to Quaternary, caused the breaching of the seal and the leaking of the  
650 hydrocarbons previously accumulated in the Santa Cruz petroleum system. Most of the  
651 deformation is accommodated via normal faulting and widespread fracturing, whose trends  
652 are consistent with a wrench tectonic geometry compatible with the regional tectonic settings.

653

654 **Acknowledgements**

655 We acknowledge the support of sponsoring companies of Phase 3 of the Sand Injection  
656 Research Group (SIRG). We are very grateful to David Iacopini for the critical review of the  
657 paper. We also wish to thanks Denis Bureau and Antonella Gatto for the support in the field.

658

659 **References**

660

661 Atwater, T., Stock, J., 1998. Pacific-north America plate tectonics of the Neogene  
662 southwestern United States: an update. *Int. Geol. Rev.* 40, 375-402.

663

664 Aydin, A., Page, B.M., 1984. Diverse Pliocene-Quaternary tectonics in a transform  
665 environment, San Francisco Bay region, California. *GSA Bulletin* 95, 1303-1317.

666

667 Barron, J.A., 1986. Paleooceanographic and tectonic controls on deposition of the Monterey  
668 Formation and related siliceous rocks in California. *Palaeogeography, Palaeoclimatology,*  
669 *Palaeoecology* 53, 27-45.

670

671 Boehm, A., Moore, J.C., 2002. Fluidized sandstone intrusions as an indicator of paleostress  
672 orientation, Santa Cruz, California. *Geofluids* 2, 147-161.

673

674 Brabb, E.E., 1989. Geologic map of Santa Cruz County, California: U.S. Geological Survey  
675 Miscellaneous Investigations Series Map I-1905, scale 1:62,500 (1 sheet).

676

677 Bradley, W.C., Griggs, G.B., 1976. Form, genesis, and deformation of central California  
678 wave-cut platforms. Geological Society of America Bulletin 87, 433-449.

679

680 Bürgmann, R., Arrowsmith, R., Dumitru, T., McLaughlin R., 1994. Rise and fall of the  
681 southern Santa Cruz Mountains, California, from fission tracks, geomorphology, and geodesy.  
682 J. Geophys. Res. 99, 20181–20202, doi:10.1029/94JB00131.

683

684 Cartwright, J., James, D. & Bolton, A., 2003. The genesis of polygonal fault systems: a review,  
685 in: Van Rensberger, P., Hillis, R.R., Morley, C.K. (Eds.), Subsurface Sediment Mobilization.  
686 Geological Society, London, Special Publications 216, 223–243.

687

688 Cartwright, J.A., Huuse, M., Aplin, A., 2007. Seal bypass systems. AAPG Bulletin 91, 1141–  
689 1166.

690

691 Clark, J.C., Rietman, J.D., 1973. Oligocene stratigraphy, tectonics, and paleogeography  
692 southwest of the San Andreas fault, Santa Cruz Mountains and Gabilan Range, California  
693 Coast Ranges: U.S. Geological Survey Professional Paper 783, 18 p.

694

695 Clark, J.C., 1981. Stratigraphy, palaeontology, and geology of the central Santa Cruz  
696 Mountains, California Coast Range: U.S. Geological Survey Professional paper 1168, p. 51.

697

698 Delaney, P.T., Pollard, D.D., Ziony J.I., McKee E.H., 1986. Field relations between dikes and  
699 joints emplacement processes and paleostress analysis. Journal of Geophysical Research 91,  
700 4920-4938.

701

**This is a non-peer reviewed pre-print.**

The Manuscript is currently under review in Marine and Petroleum Geology. Please note the subsequent version of this manuscript may have a different content.

702 Dickinson, W.R., Ducea, M., Rosenberg, L.I., Greene, H.G., Graham, S.A., Clark, J.C.,  
703 Weber, G.E., Kidder, S., Ernst, W.G., Brabb, E.E., 2005. Net dextral slip, Neogene San  
704 Gregorio–Hosgri fault zone, coastal California: Geologic evidence and tectonic implications:  
705 Geological Society of America Special Paper 391, 43 p.. doi: 10.1130/2005.2391.

706

707 Dixon, R.J., Schofield, K., Anderton, R., Reynolds, A.D., Alexander, R.W.S., Williams, M.C.,  
708 Davies, K.G., 1995. Sandstone diapirism and clastic intrusion in the Tertiary submarine fans  
709 of the Bruce-Beryl Embayment, Quadrant 9, UKCS, in: Hartley, A.J., Prosser, D.J. (Eds.),  
710 Characterisation of deep-marine clastic systems: Geological Society, London Special  
711 Publication 94, 77–94.

712

713 Duranti, D., Hurst, A., Bell, C., Groves, S., Hanson, R. 2002. Injected and remobilised Eocene  
714 sandstones from the Alba Field, UKCS: core and wireline log characteristics. *Petrol. Geosci.*  
715 8, 99–107.

716

717 Duranti, D., Hurst, A., 2004. Fluidization and injection in the deep-water sandstones of the  
718 Eocene Alba formation (UK north Sea). *Sedimentology* 51, 503-529.

719

720 Eldridge, G.H., 1901. The asphalt and bituminous rock deposits of the United States: U.S.  
721 Geological Survey Ann. Rept. 22, pt. 1, 209-464.

722

723 El-Sabbagh, D., Garrison, R.E., 1990. Silica digenesis in the Santa Cruz Mudstone (Upper  
724 Miocene), La Honda Basin, California, in: Garrison, R.E., Greene, H.G., Hicks, K.R., Weber  
725 G.E., Wright T.L. (Eds.), *Geology and Tectonics of the Central California Coast Region*, San

**This is a non-peer reviewed pre-print.**

The Manuscript is currently under review in Marine and Petroleum Geology. Please note the subsequent version of this manuscript may have a different content.

726 Francisco to Monterey, Volume and Guidebook, Pacific Sec. Assoc. Amer. Petrol. Geol., 123–  
727 132.

728

729 Ferre', E.C., Galland, O., Montanari, D., Kalakay, T.J., 2012. Granite magma migration and  
730 emplacement along thrusts. Int. J. Earth Sci. Geol. Rundschau Springer.  
731 <http://dx.doi.org/10.1007/s00531-012-0747-6>.

732

733 Galland, O., De Bremond d'Ars, J., Cobbold, P.R., Hallot, E., 2003. Physical models of  
734 magmatic intrusion during thrusting. Terra Nova 15, 405-409.

735

736 Galland, O., Cobbold, P.R., De Bremond d'Ars, J., Hallot, E., 2007. Rise and emplacement  
737 of magma during horizontal shortening of the brittle crust: insights from experimental  
738 modelling. J. Geophys. Res. 112, B06402. [http:// dx.doi.org/10.1029/2006JB004604](http://dx.doi.org/10.1029/2006JB004604).

739

740 Hallmark, R.O., 1980. Unconventional petroleum resources in California: Calif. Div. Oil  
741 and Gas Pub. TR25, 17 p.

742

743 Heck, R.G., Edwards, E.B., Kronen, J.D., Jr., Willingham, C., 1990. Petroleum potential of  
744 the offshore outer Santa Cruz and Bodega basins, California, in: Garrison, R.E., Greene, H.G.,  
745 Hicks, K.R., Weber, G.E., Wright, T.L. (Eds.), Geology and tectonics of the Central California  
746 Coast Region—San Francisco to Monterey. American Association of Petroleum Geologists,  
747 Pacific Section, Calif., 143-163.

748

749 Hosford Scheirer, A., Magoon, L.B., Graham, S.A., 2013. Petroleum Systems of the Santa  
750 Cruz County Coast, California. AAPG Search and Discovery Article, Pacific Section AAPG,  
751 SPE and SEPM Joint Technical Conference, Monterey, California.

752

753 Hurst, A., Cartwright, J.A., Duranti, D., Huuse, M., Nelson, M., 2005. Sand injectites: an  
754 emerging global play in deep-water clastic environments, in: Doré, A., Vining, B. (Eds.),  
755 Petroleum Geology: North-west Europe and Global Perspectives. Proceedings of the 6<sup>th</sup>  
756 Petroleum Geology conference. Geological Society, London, 133–144.

757

758 Hurst, A., Cartwright, J.A., Huuse, M., Duranti, D., 2006. Extrusive sandstones (extrudites):  
759 a new class of stratigraphic trap?, in: Allen, M.R., Goffey, G.R, Morgan, R.K., Walker, I.M.  
760 (Eds.), The deliberate search for the stratigraphic trap. Geological Society, London, Special  
761 Publications 254, 289-300.

762

763 Hurst, A., Scott, A., Vigorito, M., 2011. Physical characteristics of sand injectites. Earth Sci.  
764 Rev. 106, 215-246.

765

766 Hurst, A., Vigorito M., 2017. Saucer-shaped sandstone intrusions: An underplayed reservoir  
767 target. AAPG Bulletin 101, 625–633.

768

769 Huuse, M.J., Cartwright, J.A., Hurst, A., Steinsland, N., 2007. Seismic characterization of  
770 large-scale sandstone intrusions, in: Hurst, A., Cartwright, J. (Eds.), Sand Injectites:  
771 Implications for Hydrocarbon Exploration and Production: American Association of  
772 Petroleum Geologists Memoir, Tulsa, 21–35.

773

**This is a non-peer reviewed pre-print.**

The Manuscript is currently under review in Marine and Petroleum Geology. Please note the subsequent version of this manuscript may have a different content.

774 Jackson, C.A.L., Huuse, M., Barber, G.P., 2011. Geometry of wing-like intrusions adjacent  
775 to a deep-water slope channel complex and implications for hydrocarbon exploration and  
776 production: a 3D seismic case from the Maloy Slope, offshore Norway. AAPG Bull. 95, 559-  
777 584.

778

779 Jenkins, O.P., 1930. Sandstone dikes as conduits for oil migration through shales. AAPG Bull.  
780 14, 411-421.

781

782 Jolly, R.J.H., Lonergan, L., 2002. Mechanisms and controls on the formation of sand  
783 intrusions. J. Geol. Soc. Lond. 159, 605-617.

784

785 Kim, Y., Peacock, D.C.P., Sanderson, D.J., 2004. Fault damage zones. J. Struct. Geol. 26,  
786 503-517.

787

788 Lillis, P.G., Stanley, R.G., 1999. Petroleum systems of the La Honda Basin, California. AAPG  
789 Bulletin 83, 694-694.

790

791 Lowe, D.R., 1975. Water escape structures in coarse-grained sediments. Sedimentology 22,  
792 157-204.

793

794 Manzocchi, T., Ringrose, P.S., Underhill, J.R., 1998. Flow through fault systems in high-  
795 porosity sandstones, in: Coward, M.P., Daltaban, T.S., Johnson, H. (Eds.), Structural Geology  
796 in Reservoir Characterization. Geological Society, London, Special Publications 127, 65-82.

797

**This is a non-peer reviewed pre-print.**

The Manuscript is currently under review in Marine and Petroleum Geology. Please note the subsequent version of this manuscript may have a different content.

798 Manzocchi, T., 2002. The connectivity of two-dimensional networks of spatially correlated  
799 fractures, *Water Resour. Res.* 38, 1162. doi:10.1029/2000WR000180

800

801 Molyneux, S., 1999. Giant clastic dykes and sills of Santa Cruz, Coastal California. *Petroleum*  
802 *Exploration Society of Great Britain, Newsletter*, 118–125.

803

804 Moody, J.D; Hill, M.J., 1956. Wrench-fault tectonics. *GSA Bulletin* 67, 1207-1246.

805

806 Mullins, H.T., Nagel, D.K., 1982. Evidence for shallow hydrocarbons offshore northern Santa  
807 Cruz County, California. *Bull. Am. Assoc. Pet. Geol.* 66, 1130-1140.

808

809 Newsom, J.F., 1903. Clastic dikes. *Geological Society of America Bulletin* 14, 227–268.

810

811 Page, B.M., Holmes, C.N., 1945. Geology of the bituminous sandstone deposits near Santa  
812 Cruz County, California: U.S. Geological Survey Oil and Gas Investigations Preliminary Map  
813 27.

814

815 Page, B.M., Thompson, G.A., Coleman, R.G., 1998. Late Cenozoic tectonics of the central  
816 and southern coast ranges of California. *Geol. Soc. Am. Bull.* 110, 846-876.

817

818 Palladino, G., Grippa, A., Bureau, D., G. Ian, Alsop, Hurst, A., 2016. Emplacement of  
819 sandstone intrusions during contractional tectonics. *Journal of Structural Geology* 89, 230-  
820 249.

821

**This is a non-peer reviewed pre-print.**

The Manuscript is currently under review in Marine and Petroleum Geology. Please note the subsequent version of this manuscript may have a different content.

822 Palladino, G., G. Ian, Alsop, Grippa, A., Zvirtes G., Philipp R.P., Hurst, A., 2018. Sandstone-  
823 filled normal faults: A case study from central California. *Journal of Structural Geology* 110,  
824 86–101.

825

826 Peacock, D.C.P., Nixon, C.W., Rotevatn, A., Sanderson, D.J., Zuluaga, L.F., 2016. Glossary  
827 of fault and other fracture networks. *Journal of Structural Geology* 92, 12-29.

828

829 Phillips, R.L., 1981. Depositional and structural controls on heavy-petroleum tar sands in  
830 Santa Cruz Mountains. *AAPG Bull.* 65. p. 970.

831

832 Phillips, R.L., 1990. Depositional and structural controls on the distribution of tar sands in the  
833 Santa Cruz mountains, California, in: Garrison, R, Greene, H.G., Hicks, K.R., Weber, G.E.,  
834 Wright, T.L. (Eds.), *Geology and Tectonics of the Central California Coastal Region, San*  
835 *Francisco to Monterey, Volume and Guidebook, Pacific Section, American Association of*  
836 *Petroleum Geologists, Pacific Section, Bakersfield, CA, Book GB67, 105–21.*

837

838 Phizackerley, P.H., Scott, L.O., 1978. Major tar-sand deposits of the world, in: Chilingarian,  
839 G.V., (Ed.), *Bitumens, Asphalts, and Tar Sands, 57-92.*

840

841 Rizzo, R.E., Healy, D., De Siena, L., 2017. Benefits of maximum likelihood estimators for  
842 fracture attribute analysis: Implications for permeability and up-scaling. *Journal of Structural*  
843 *Geology* 95, 17-31.

844

**This is a non-peer reviewed pre-print.**

The Manuscript is currently under review in Marine and Petroleum Geology. Please note the subsequent version of this manuscript may have a different content.

845 Scott, A., Vigorito, M., Hurst, A., 2009. The process of sand injection: internal structures and  
846 relationships with host strata (Yellowbank Creek Injectite Complex, California, U.S.A.).  
847 *Journal of Sedimentary Research* 79, 568–583.

848

849 Scott, A., Hurst, A., Vigorito, M., 2013. Outcrop-based reservoir characterization of a  
850 kilometer-scale sand-injectite complex. *AAPG Bull.* 97, 309-343.

851

852 Sherry, T.J., Rowe, C.D., Kirkpatrick, J.D., Brodsky, E.E., 2012. Emplacement and  
853 dewatering of the world’s largest exposed sand injectite complex. *Geochemistry, Geophysics,*  
854 *Geosystems* 13, 1-17.

855

856 Sibson, R.H., 1996. Structural permeability of fluid-driven fault-fracture meshes. *Journal of*  
857 *Structural Geology* 18, 1031-1042.

858

859 Stanley, R.G., McCaffrey, R., 1983. Extent and offset history of the Ben Lomond Fault, Santa  
860 Cruz County, California, In: Andersen, D.W., Rymer, M.J. (Eds.), *Tectonics and*  
861 *Sedimentation Along Faults of the San Andreas System*. SEPM—Society of Economic  
862 *Paleontologists and Mineralogists*, Los Angeles, California, 79– 90.

863

864 Stanley, R.G., 1990. Evolution of the Tertiary La Honda Basin, central California, in:  
865 Garisson, R.E. et al. (Eds.), *Geology and Tectonics of the Central California Coastal Region,*  
866 *San Francisco to Monterey*, Guidebook, Am. Assoc. of Pet. Geol., Bakersfield, Calif., 67, 1–  
867 29.

868

**This is a non-peer reviewed pre-print.**

The Manuscript is currently under review in Marine and Petroleum Geology. Please note the subsequent version of this manuscript may have a different content.

869 Thompson, B.J., Garrison, R.E., Moore, J.C., 1999. A late Cenozoic sandstone intrusion west  
870 of Santa Cruz, California: Fluidized flow of water- and hydrocarbon saturated sediments, in:  
871 Garrison, R.E. Aiello I.W., Moore, J.C. (Eds.), Late Cenozoic fluid seeps and tectonics along  
872 the San Gregorio fault zone in the Monterey Bay region, California: Pacific Section AAPG  
873 Volume and Guidebook GB-16, p. 53–74.

874

875 Thompson, B.J., Garrison, R.E., Moore, C.J., 2007. A reservoir-scale Miocene Injectite near  
876 Santa Cruz, California, in: Hurst, A., Cartwright, J. (Eds.), Sand Injectites: Implications for  
877 Hydrocarbon Exploration and Production: American Association of Petroleum Geologists,  
878 Memoir 87, 151–162.

879

880 Vigorito, M., Hurst, A., Cartwright, J., Scott, A., 2008. Regional-scale shallow crustal  
881 remobilization: processes and architecture. Geol. Soc. Lond. Spec. Publ. 165, 609-612.

882

883 Vigorito, M., Hurst, A., 2010. Regional sand injectite architecture as a record of pore pressure  
884 evolution and sand redistribution in the shallow crust: insights from the Panoche Giant  
885 Injection Complex, California. J. Geol. Soc. Lond. 167, 889-904.

886

887 Weber, G.E., Allwardt, A.O., 2001. The geology from Santa Cruz to Point Año Nuevo: The  
888 San Gregorio fault zone and Pleistocene marine terraces: U.S. Geological Survey Bulletin,  
889 2188, p. 1–32.

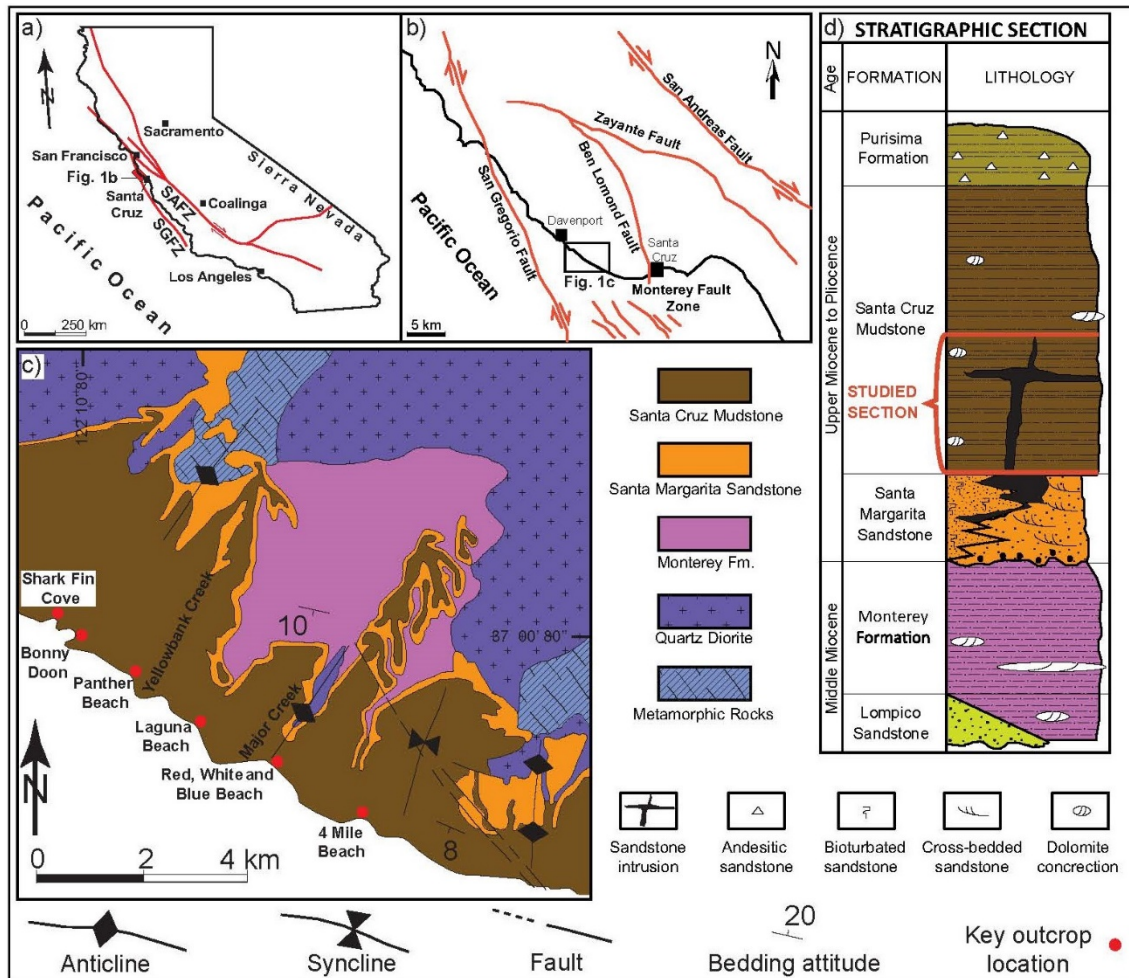
890

891 Wilcox, R.E., Harding, T.P., Seely, D.R. 1973. Basic Wrench Tectonics. AAPG Bulletin 57,  
892 74-96.

893

894

Figures



895

896

897

898

899

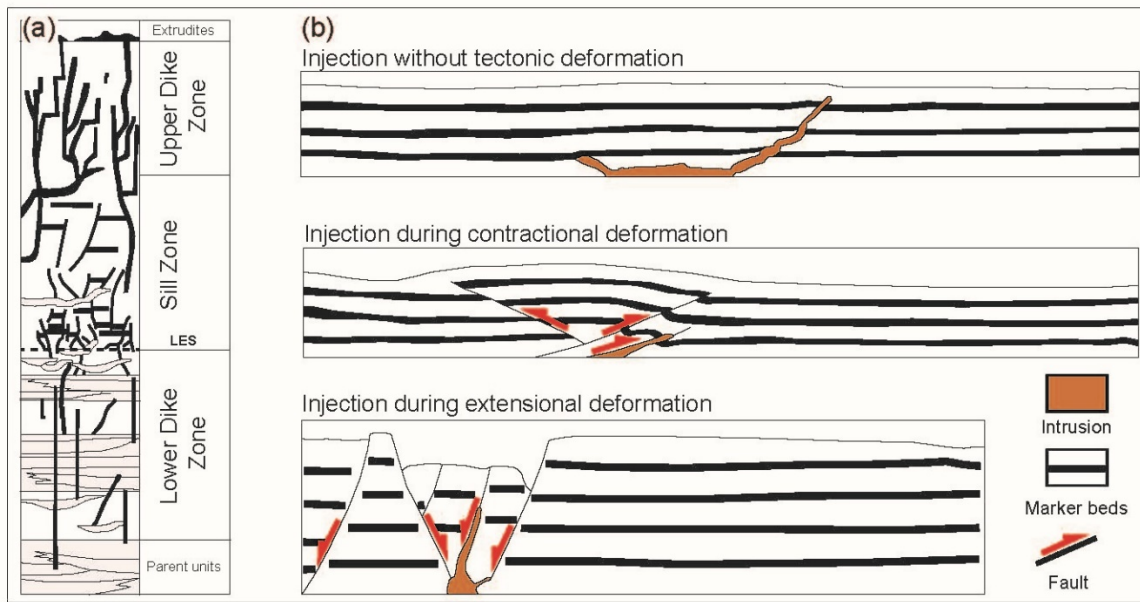
900

901

902

903

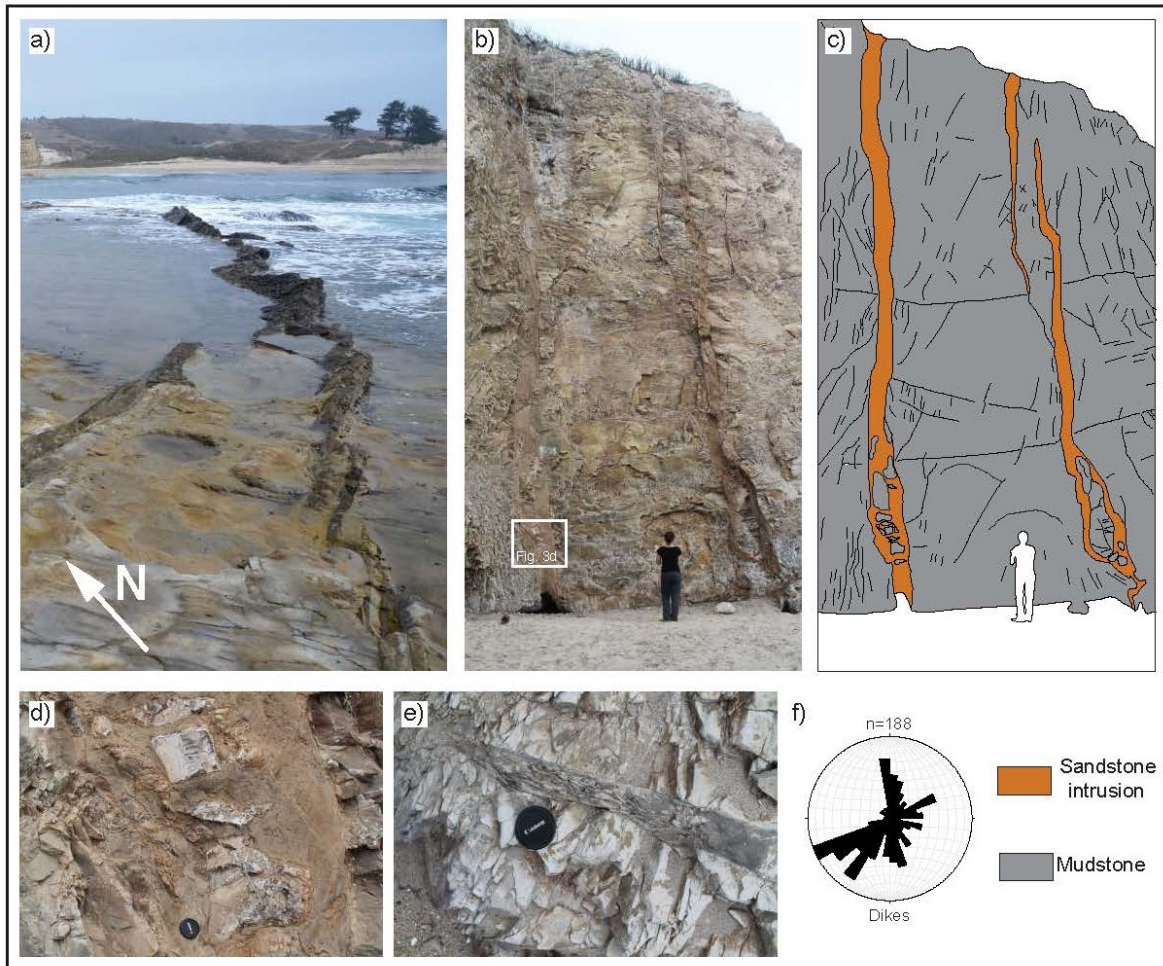
Fig. 1 a) Sketch map of California including the location of the study area (red box) and the main tectonic structures represented by the San Andreas Fault Zone (SAFZ) and the San Gregorio Fault Zone (SGFZ). b) Schematic structural map. The study area is included between the Ben Lomond and the San Gregorio fault zones. c) Geological map of the study area (modified from Boehm and Moore, 2002). Outcrop locations and places referred to in the text are also shown. d) Stratigraphic column of the geological units cropping out in the Santa Cruz coastal area (modified from Boehm and Moore, 2002).



904

905 Fig. 2 a) Schematic organization of a sandstone intrusion complex following Vigorito and  
906 Hurst (2010). Dikes mainly occur in the lower and upper portion of the sequence. Sills are  
907 common in the middle portion. b) Possible geometry obtained for tectonically-unrelated and  
908 tectonically-controlled intrusions from laboratory experiments (modified from Galland et al.,  
909 2007).

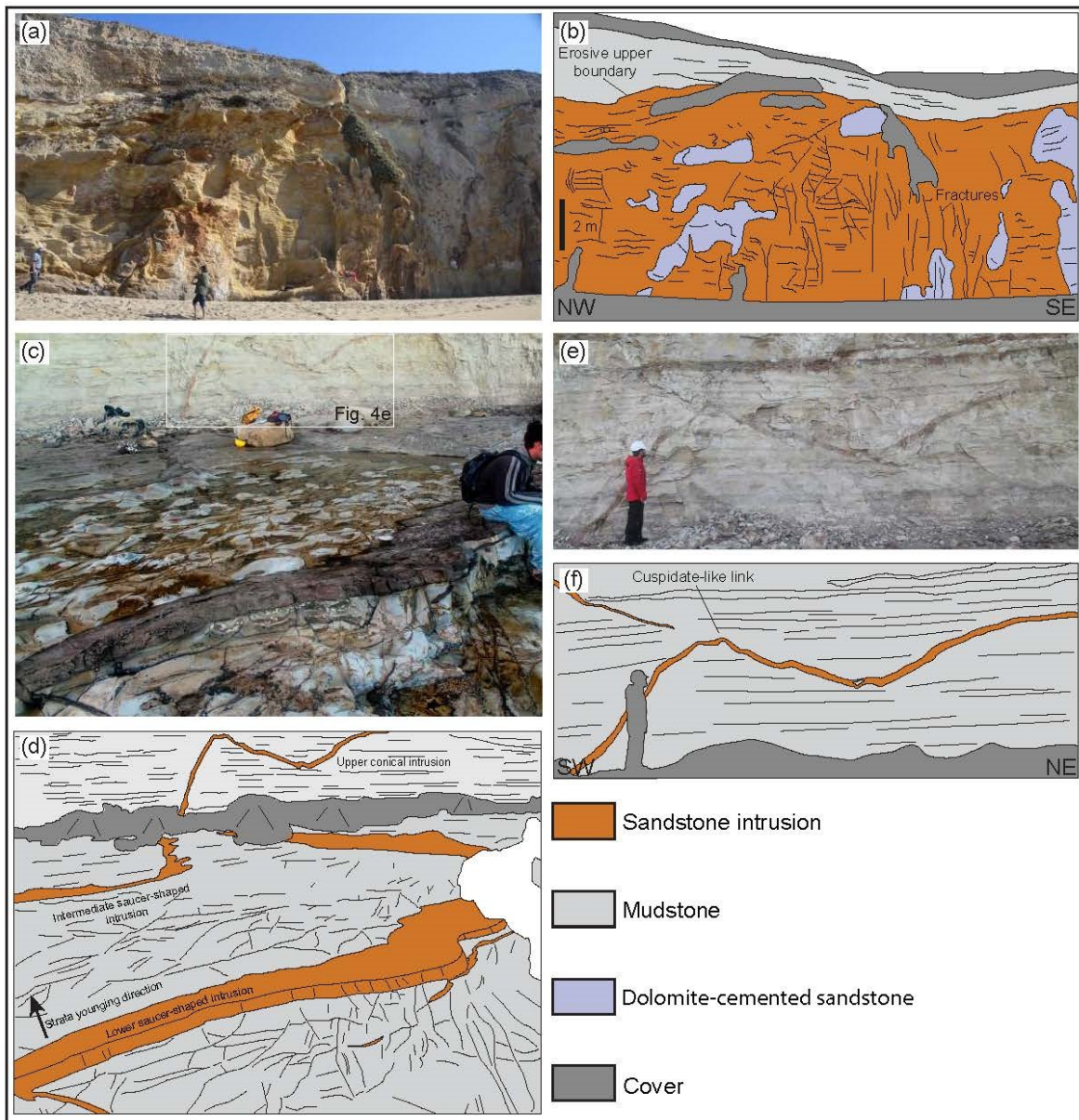
910



911

912 Fig. 3. Main characteristics of the dikes forming the SCIC. a) Bifurcating dike exposed at low  
913 tide in 4 Mile Beach. b) Photograph and interpretative line drawing (c) of dike swarm  
914 observable at Bonny Doon Beach. Note the local side-stepping geometry and the occurrence  
915 of decimetre to metre scale mud-clasts. d) Close up view of mud-clasts contained in the  
916 previous dike. e) Cm-scale mud-clasts contained in a tar saturated dike at Bonny Doon Beach.  
917 Note the clast orientation probably acquired during emplacement of the sandstone intrusion.  
918 f) Rose diagram showing dike orientations in the Santa Cruz coastal area. Preferential N-S,  
919 WSW-ENE and SW-NE trends are evident.

920

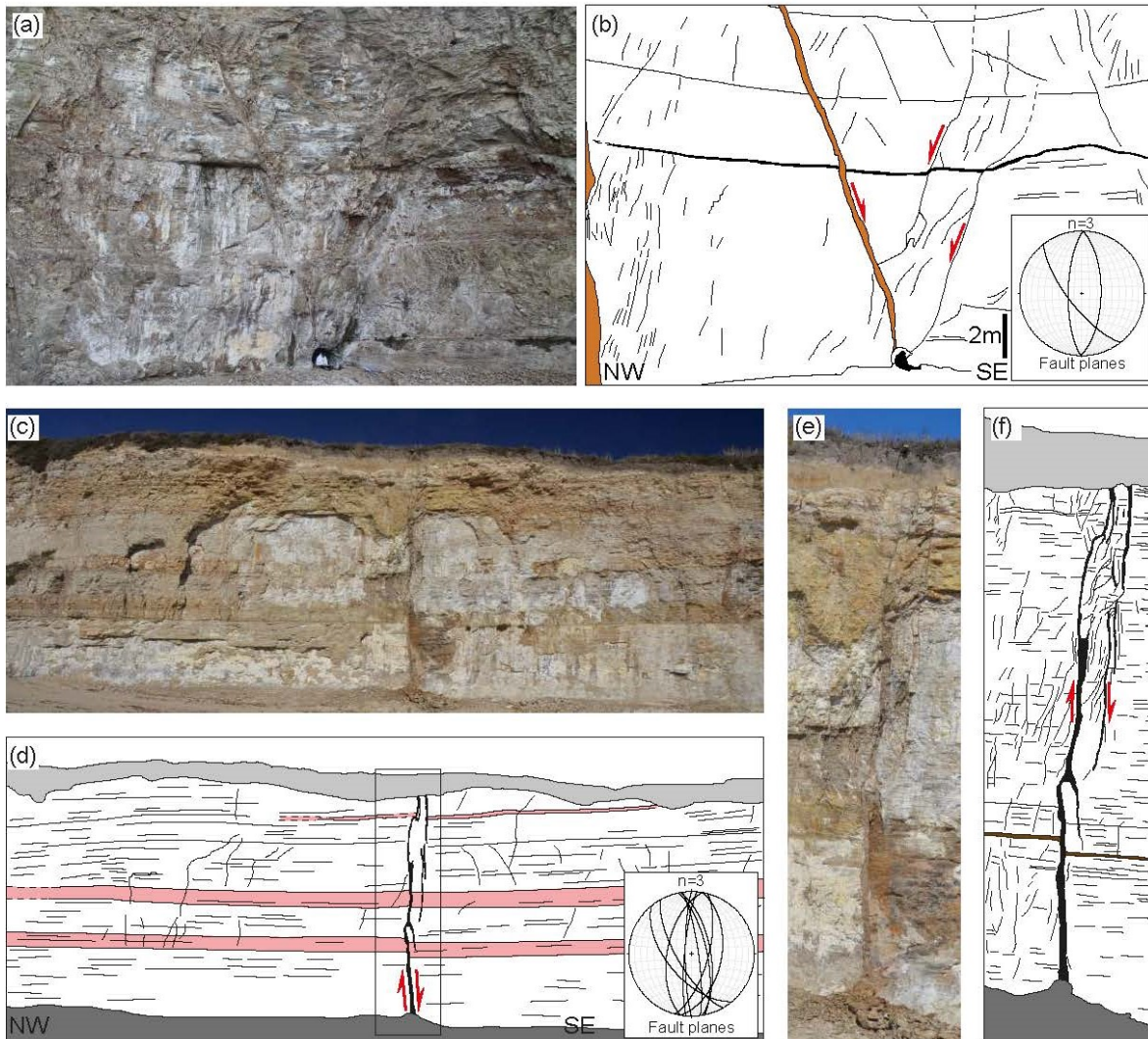


921

922 Fig. 4. Main characteristics of sills and saucer-shaped intrusions forming the SCIC. a)  
923 Photograph and interpretative line drawing (b) of a sill cropping out at Panther Beach  
924 characterized by a marked upper erosional boundary. Internal structures are clearly visible and  
925 are represented by plane-parallel and convolute lamination. Note also arrays of near-vertical  
926 fractures cross-cutting the sandstone body. c) Photograph and interpretative line drawing (d)  
927 of nested tar-saturated saucer-shaped intrusions recognised at different stratigraphic levels in  
928 the Santa Cruz mudstone at 4 Mile Beach. e) Photograph and interpretative line drawing (f)  
929 of cross-section of a conical sandstone intrusion cropping out at 4 Mile Beach. Note that this

930 sandstone body is connected with the underlying sandstone intrusion through a dike forming  
931 a cuspidate-shaped geometry.

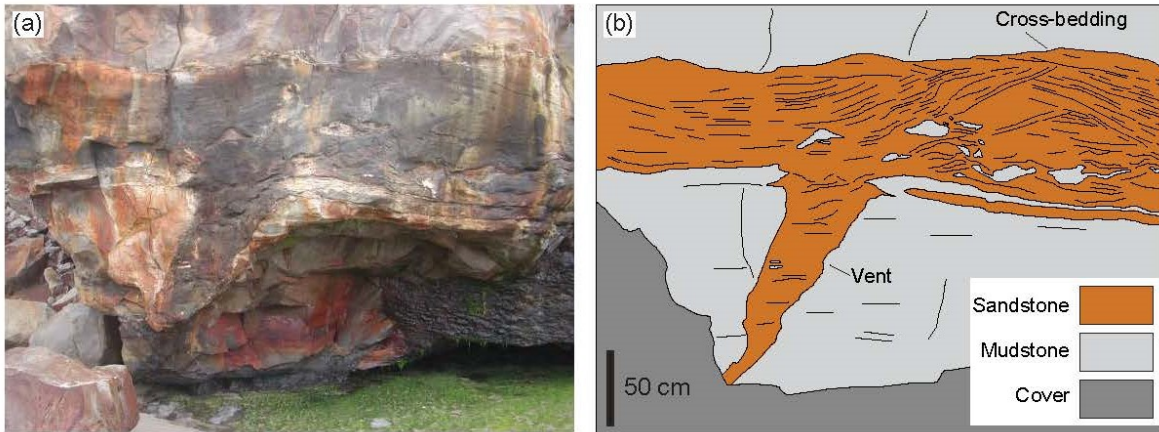
932



933

934 Fig. 5. Main characteristics of sandstone-filled faults forming the SCIC. a) Photograph and  
935 interpretative line drawing (b) of a conjugate set of N-S and NNW-SSE faults recognised at  
936 Bonny Doon. The amount of offset, up to 15 cm, is provided by a dark marker clay level. c)  
937 Photograph and interpretative line drawing (d) of sandstone-filled normal fault recognised at  
938 Laguna Creek Beach. e) Photograph and interpretative line drawing (f) of detail from the  
939 previous outcrop. Note the complex structure of the fault plane and the sandstone intruded  
940 within even the thinnest fault segments.

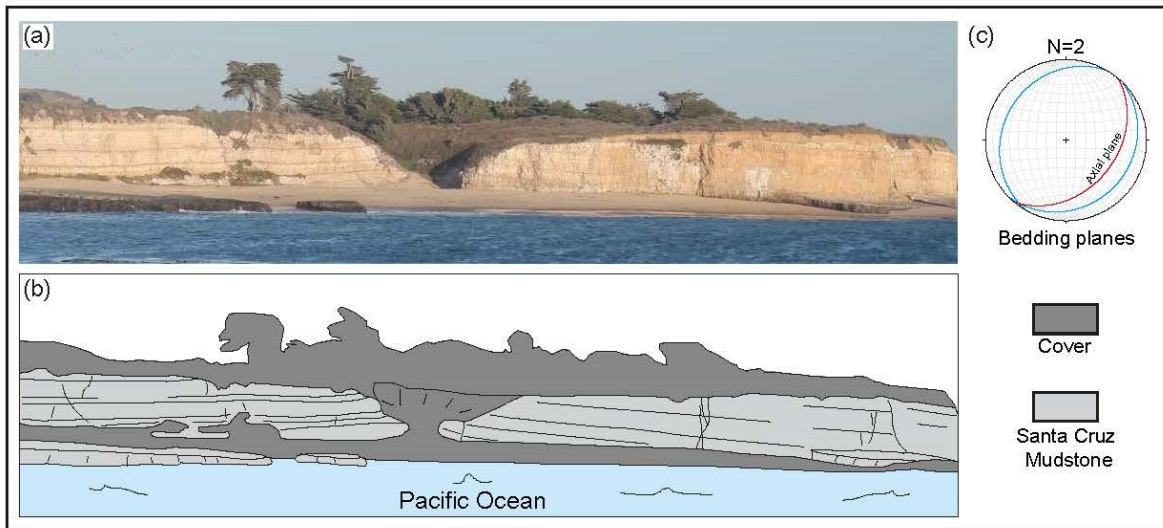
941



942

943 Fig. 6. Main characteristics of extrudites forming the SCIC at Red, White and Blue Beach. a)  
944 Photograph and interpretative line drawing (b) of bed-parallel, mound-shaped extrudite  
945 displaying cross-bedding and isolated mud-clasts ripped up from the host strata. Note the  
946 underlying vent feeding the extrudite. The dark colour of the sandstone is attributable to the  
947 occurrence of tar.

948

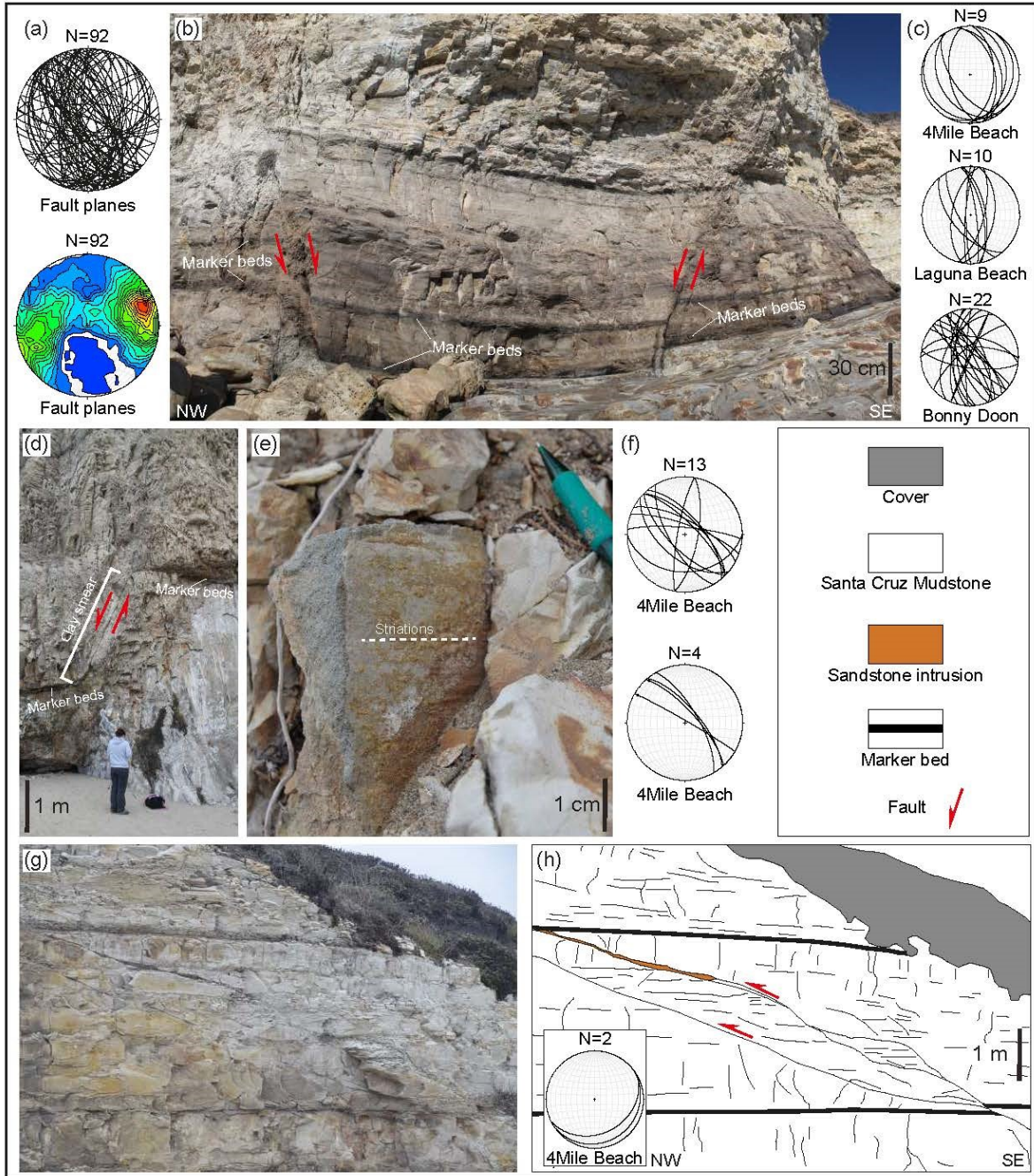


949

950 Fig. 7. a) Photograph and interpretative line drawing (b) of NW-SE trending open fold  
951 deforming the Santa Cruz Mudstone at 4 Mile Beach. Note that the recent fluvial incision  
952 closely corresponds with the fold hinge zone where outer arc extension fracturing took place.

953 c) Lower hemisphere equal area stereographic projection showing the orientation of the fault  
954 limbs and the resulting axial planes (great circles).

955



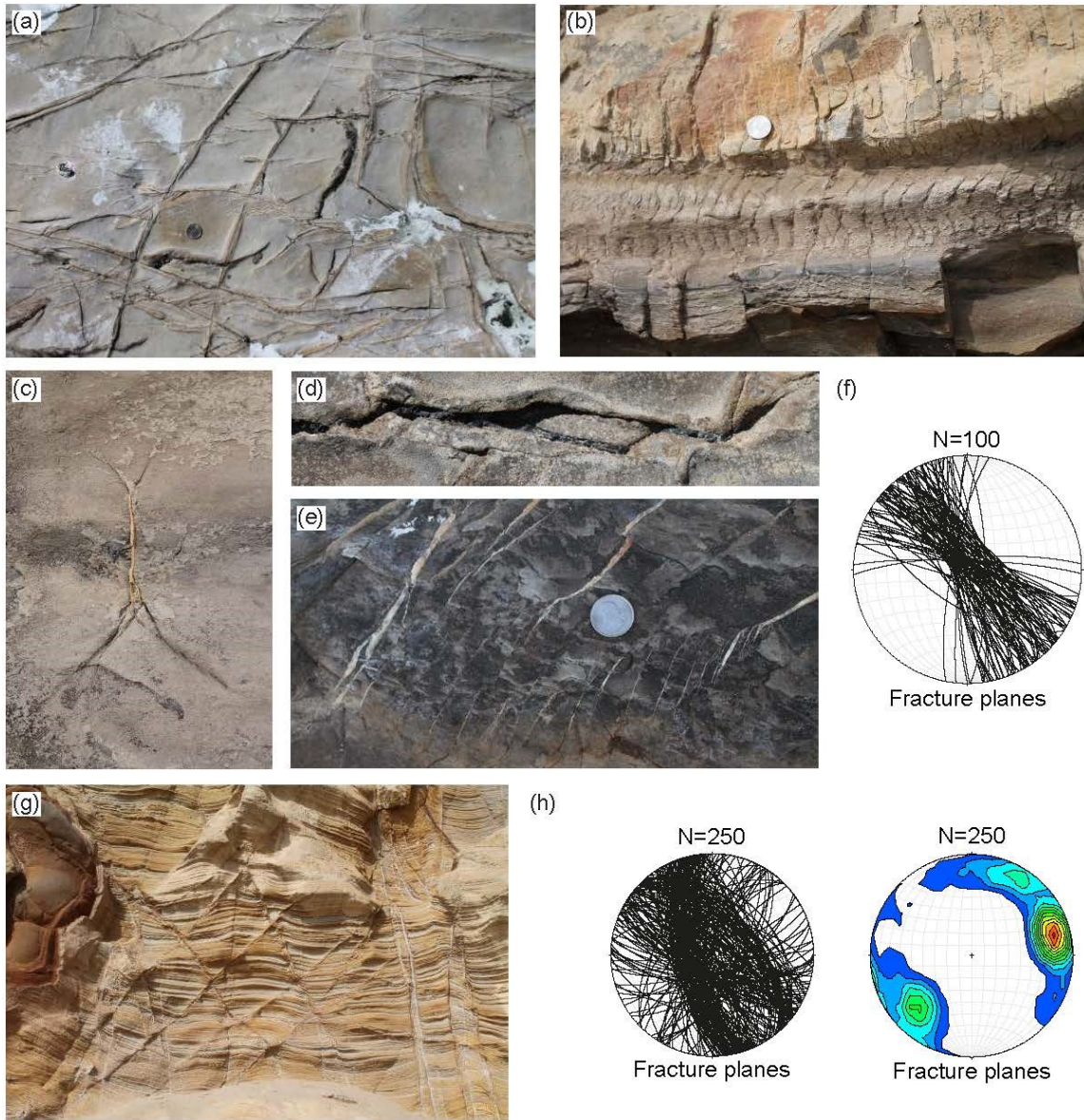
956

957 Fig. 8. a) Preferential orientations of faults recognised along the Santa Cruz coastal area. Note  
958 that faults shown on stereoplots are dominantly NNW-SSE and N-S trending. b) Conjugate  
959 normal faults forming a NNW-SSE trending graben in 4 Mile Beach. The measured amount  
960 of the offset, about 20 cm, is based on the displacement of dark maker beds alternating to the

**This is a non-peer reviewed pre-print.**

The Manuscript is currently under review in Marine and Petroleum Geology. Please note the subsequent version of this manuscript may have a different content.

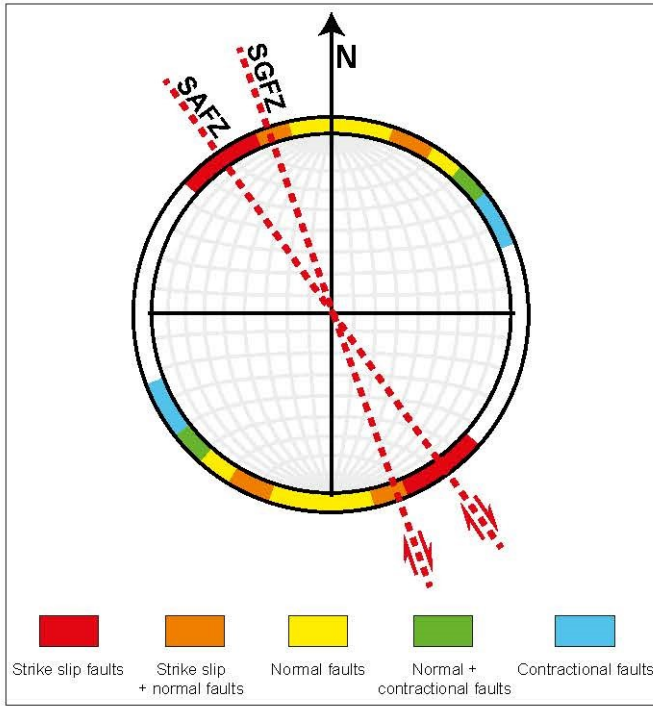
961 Santa Cruz Mudstone. c) Lower hemisphere equal area stereographic projections showing the  
962 orientation of the normal fault planes (great circles) in some key outcrops recognised along  
963 the investigated area. d) Normal fault showing smeared clay along the fault surface at Bonny  
964 Doon Beach. e) Striated strike slip fault exploiting a pre-existent discontinuity represented by  
965 the boundary between a sandstone intrusion and the Santa Cruz Mudstone at 4 Mile Beach. f)  
966 Lower hemisphere equal area stereographic projections showing the orientation of strike-slip  
967 faults (great circles) in some key outcrops recognised along the investigated area. g) Reverse  
968 faults recognised at 4 Mile Beach. Note the occurrence of tar-saturated injected sandstone  
969 within dilational jogs occurring along the fault plane. h) Line drawing interpretation.  
970



971

972 Fig. 9. a) Details of the fracture network affecting the Santa Cruz Mudstone observable in  
973 plan view at 4 Mile Beach. b) S-shaped fractures and c) fracture meshes recognised at 4 Mile  
974 Beach. Note the occurrence of calcite within the fractures. d) Tar-saturated fracture recognised  
975 at 4 Mile Beach. e) Calcite-filled, *en-echelon* fractures at 4 Mile Beach. f) Lower hemisphere  
976 equal area stereographic projections showing the orientation of fractures (great circles) at 4  
977 Mile Beach. g) Sets of conjugate fractures cutting through sandstone intrusions at Panther  
978 Beach. Note the resulting honeycomb structure. h) Lower hemisphere equal area stereographic  
979 projections showing the orientation of fractures (great circles) at Panther Beach.

980



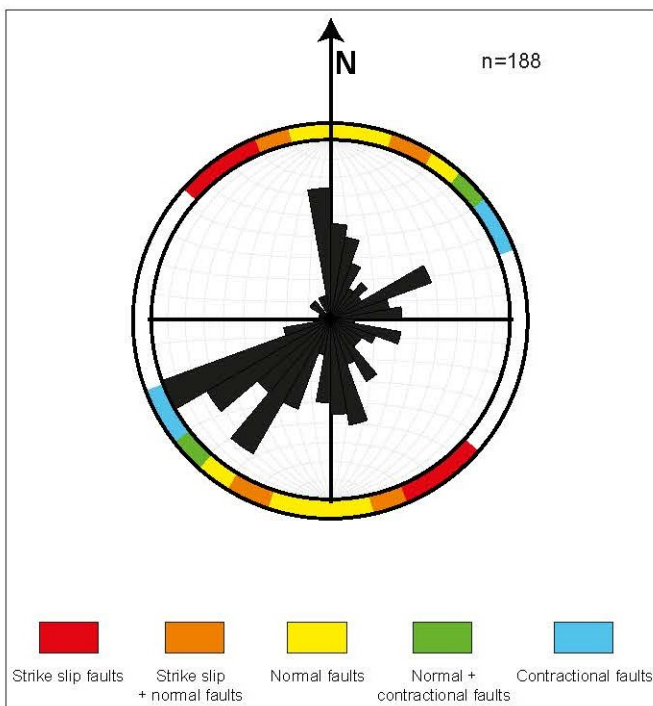
981

982

Fig. 10. Diagram showing the main range of trends of the tectonic structures recognised in the Santa Cruz Coastal area. The trends of the San Andres and San Gregorio fault zones are also included (red dotted lines).

984

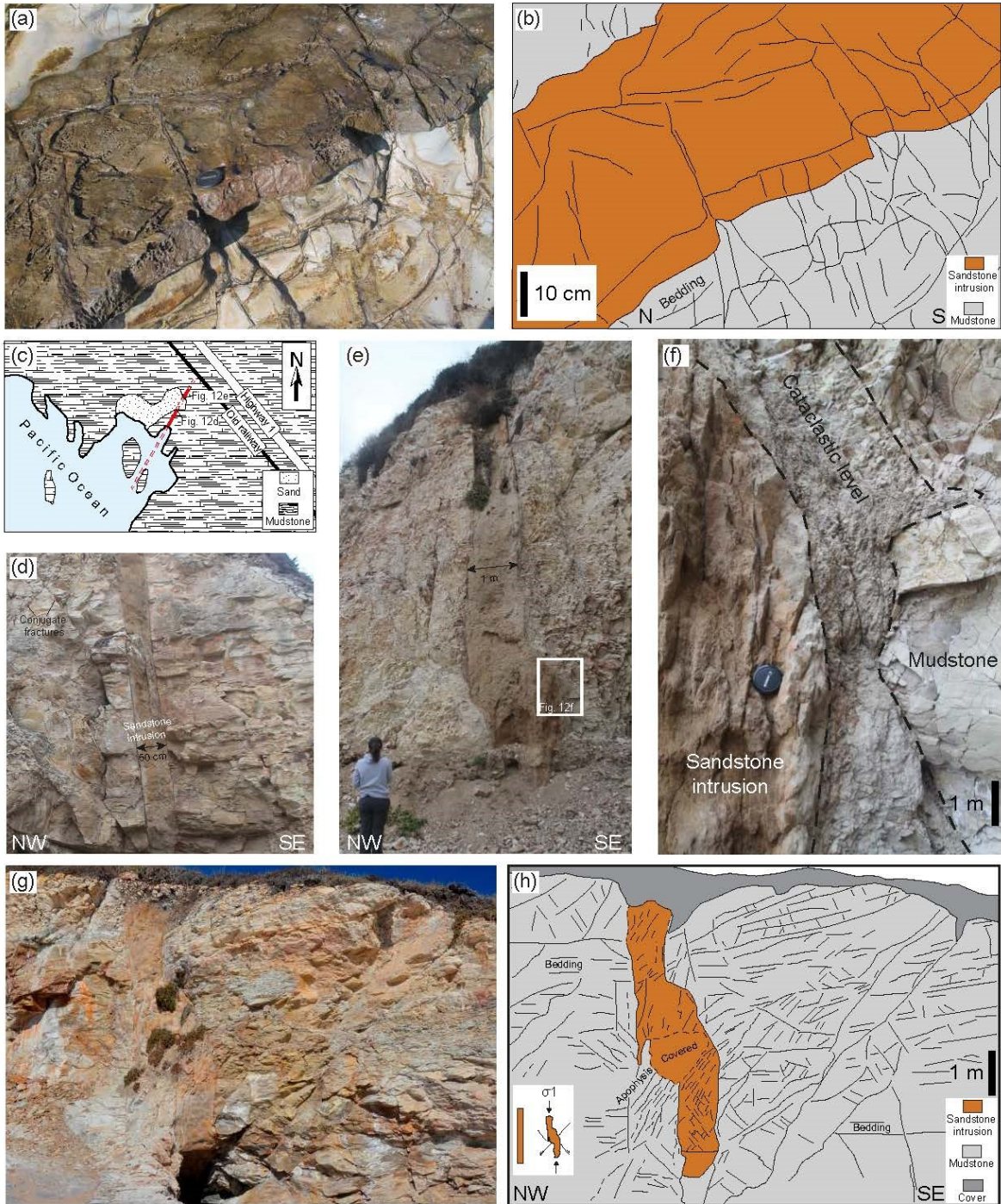
985



986

987 Fig. 11. Diagram showing the main relationships between dike orientations and fault and  
988 fracture patterns. Note that most dikes have been emplaced along extensional structures.

989



990

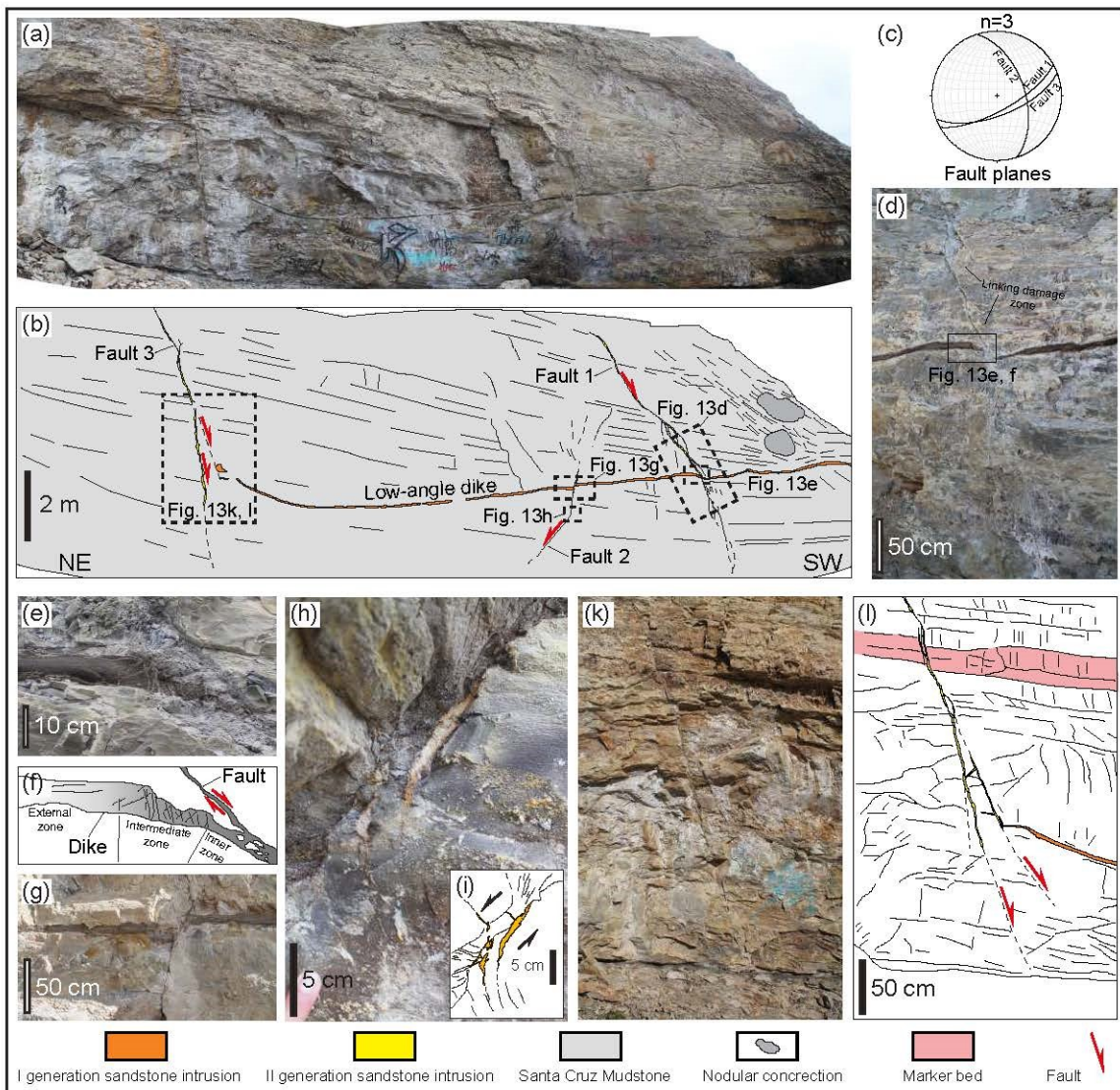
991 Fig. 12. Evidence for tectonic overprint of sandstone intrusions along the Santa Cruz coastal

992 area. a) Photograph and interpretative line drawing (b) of 10 cm-thick sills overprinted by

**This is a non-peer reviewed pre-print.**

The Manuscript is currently under review in Marine and Petroleum Geology. Please note the subsequent version of this manuscript may have a different content.

993 fractures recognised at 4 Mile Beach. Observable mechanical discontinuities mainly consist  
994 of fractures nearly orthogonal to the sill-host mudstone interface and bedding surfaces. Sill-  
995 parallel fractures are notably lacking. c) Sketch map of Shark Fin Cove with the sandstone  
996 intrusion shown in red. d) Portion of the considered sandstone intrusion scarcely affected by  
997 later tectonic deformation. Conjugate fractures are visible in the host strata but, importantly,  
998 do not affect the dike-host-strata interface. e) Same dike in a sector characterized by strong  
999 post-emplacement deformation probably related to a normal fault zone. The deformed dike  
1000 shows steps and thickened sections due to vertical compression. Most of the deformation is  
1001 focussed along the dike-host-strata interface where a thick unit of cataclastic material forms.  
1002 f) Photograph and interpretative line drawing (g) of a dike affected by post emplacement  
1003 deformation recognised at Laguna Creek Beach. Similar to the previous example, vertical  
1004 compression is accommodated by conjugate fractures, stepped geometry and thickening in the  
1005 central portion of the dike.  
1006



1007

1008

1009

1010

1011

1012

1013

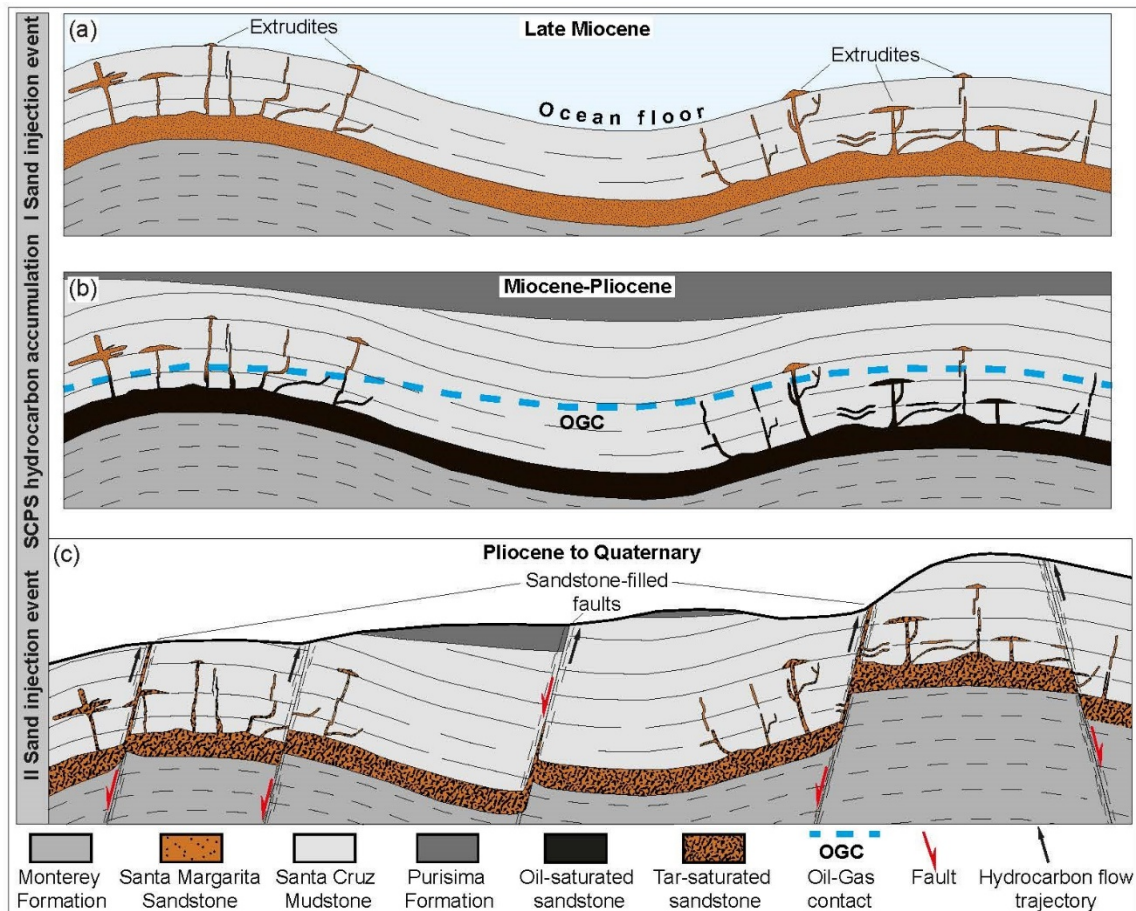
1014

1015

1016

Fig. 13. a) Photograph and interpretative line drawing (b) of cross-cutting relationships between the two recognised generations of sandstone intrusions at Panther Beach. c) Lower hemisphere equal area stereographic projections (great circles) showing the orientation of the conjugate sandstone-filled normal faults recognised at Panther Beach. d) Fault 1 shows a cm-scale offset and is only partially filled by sand. e) Close-up of Fault 1 showing the younger generation of sandstone intrusions emplaced along the fault plane, and the low-angle dike belonging to the older generation that is fractured and thinned in the proximity of the fault plane. Line drawing interpretation showing fracture distribution along the low-angle dike with respect to the distance from the fault plane. f) Photograph of Fault 2. g) *En echelon* dilation

1017 fractures partially filled by fluidised sand recognised along the Fault 2. h) Line drawing  
 1018 interpretation. i) Photograph and k) interpretation of Fault 3.  
 1019



1020  
 1021 Fig. 14. Evolutionary model proposed to explain the occurrence of the Santa Cruz Injection  
 1022 Complex and the Santa Cruz petroleum system. a) The Santa Cruz Injection Complex  
 1023 emplacement mainly occurred during the Late Miocene following a contractional deformation  
 1024 stage affecting the Santa Cruz sedimentary succession. Sand remobilization and emplacement  
 1025 related to the first sand injection event was particularly intense in the correspondence of the  
 1026 anticlines where fluid overpressure generated by the squeezing of the Santa margarita  
 1027 Sandstone and fracturing promoted by outer arc extension created suitable conditions. The  
 1028 age of the sandstone intrusion event is constrained to the Late Miocene by the extrudites  
 1029 recognised in the study area. b) The unconsolidated state of the Santa Cruz Mudstone and the

**This is a non-peer reviewed pre-print.**

The Manuscript is currently under review in Marine and Petroleum Geology. Please note the subsequent version of this manuscript may have a different content.

1030 successive accumulation of sediments at the top of the sandstone intrusion complex caused  
1031 the resealing of the system and favoured the accumulation of hydrocarbons pertaining to Santa  
1032 Cruz petroleum system in the newly-formed sandstone network between the Late Miocene  
1033 and the Early Pliocene. c) Uplift and faulting related to the Pliocene-Quaternary strike-slip  
1034 tectonic evolution of the area caused the definitive failure of the Santa Cruz petroleum system.  
1035 Tar-saturated sandstones are what remain of this petroleum system.